FIELD ORIENTED CONTROL OF INDUCTION MOTOR BY METAHEURISTIC METHODS

2023
MASTER THESIS
ELECTRICAL AND ELECTRONICS ENGINEERING

Hersh Hasan Taha AL-DAWOODI

Thesis Advisor
Assist. Prof. Dr. Hilmi AYGÜN

FIELD ORIENTED CONTROL OF INDUCTION MOTOR BY METAHEURISTIC METHODS

Hersh Hasan Taha AL-DAWOODI

Thesis Advisor

Assist. Prof. Dr. Hilmi AYGÜN

T.C.

Karabuk University

Institute of Graduate Programs

Department of Electrical and Electronics Engineering

Prepared as

Master Thesis

KARABUK

January 2023

I certify that in my opinion the thesis submitted by Hersh Hasan Taha AL-DAWOODI titled “FIELD ORIENTED CONTROL OF INDUCTION MOTOR BY METAHEURISTIC METHODS” is fully adequate in scope and quality as a thesis for the degree of Master of Science.

Assist. Prof. Dr. Hilmi AYGÜN .....
Thesis Advisor, Department of Mechatronic Engineering

This thesis is accepted by the examining committee with a unanimous vote in the Department of Electrical and Electronics Engineering as a Master of Science thesis. January 16, 2023

Examining Committee Members (Institutions)	Signature
Chairman : Assoc. Prof. Dr. Hüseyin Oktay ERKOL (BANU)	.....
Member : Assist. Prof. Dr. Mehmet ŞİMŞİR (KBU)	.....
Member : Assist. Prof. Dr. Hilmi AYGÜN (KBU)	.....

The degree of Master of Science by the thesis submitted is approved by the Administrative Board of the Institute of Graduate Programs, Karabuk University.

Prof. Dr. Müslüm KUZU .....
Director of the Institute of Graduate Programs

"I declare that all the information within this thesis has been gathered and presented in accordance with academic regulations and ethical principles and I have according to the requirements of these regulations and principles cited all those which do not originate in this work as well."

Hersh Hasan Taha AL-DAWOODI

ABSTRACT

M. Sc. Thesis

FIELD ORIENTED CONTROL OF INDUCTION MOTOR BY METAHEURISTIC METHODS

Hersh Hasan Taha AL-DAWOODI

Karabük University
Institute of Graduate Programs
The Department of Electrical and Electronics Engineering

Thesis Advisor:
Assist. Prof. Dr. Hilmi AYGÜN
January 2023, 58 pages

Three-phase squirrel-cage induction motors (IMs) are very important machines for power applications that require high reliability, high efficiency, and robust construction. Field oriented control (FOC) is an important method for controlling the IM drives with excellent performance. Due to the accuracy, simplicity, and high reliability, indirect field-oriented control (IFOC) approach is used to control the IM in this thesis. Generally, three PI controllers are used for speed, torque, and flux control in IFOC based IM. Most of the time, the gains of these PI controllers are tuned by trial and error or Ziegler Nichols method. However, these methods cause a poor dynamic response. As a result, in this thesis, to improve the dynamic performance of IFOC based IM, some metaheuristic methods such as Particle Swarm Optimization (PSO), Grey Wolf Optimization (GWO), and Artificial Bee Colony (ABC) algorithms are used to obtain the optimal values of the PI controller

parameters. The best dynamic performance is obtained by GWO algorithm although its convergence speed is slow compared to the used other algorithms.

Key Words: Three Phase Induction Motor, Field Oriented Control, SVPWM, Matlab/ Simulink, Metaheuristic, PSO, GWO, ABC.

Science Code: 90514

ÖZET

Yüksek Lisans Tezi

ASENKRON MOTORUN METAHEURİSTİK YÖNTEMLERLE ALAN ODAKLI KONTROLÜ

Hersh Hasan Taha AL-DAWOODI

Karabük Üniversitesi
Lisansüstü Eğitim Enstitüsü
Elektrik ve Elektronik Mühendisliği Anabilim Dalı

Tez Danışmanı:
Dr. Öğr. Üyesi Hilmi AYGÜN
Ocak 2023, 58 sayfa

Üç fazlı sincap kafesli asenkron motorlar (AM), yüksek güvenilirlik, yüksek verim ve dayanıklı yapı gerektiren güç uygulamaları için çok önemli makinalardır. Alan yönlendirmeli kontrol (AYK), AM sürücülerini çok iyi bir performansla kontrol etmek için önemli bir yöntemdir. Bu tezde, doğruluğu, basitliği ve yüksek güvenilirliğine bağlı olarak dolaylı alan yönlendirmeli kontrol (DAYK) yaklaşımı AM'u kontrol etmede kullanılır. DAYK tabanlı AM'da genellikle hız, moment ve akı kontrolü için üç PI kontrolör kullanılır. Çoğu zaman, bu PI kontrolörlerin kazançları deneme-yanılma yoluyla veya Ziegler Nichols yöntemi ile ayarlanır. Fakat bu yöntemler zayıf bir dinamik performansa neden olur. Bu sebeple, bu tezde, DAYK tabanlı AM'un dinamik performansını iyileştirmek için Parçacık Sürüsü Optimizasyonu (PSO), Gri Kurt Optimizasyonu (GKO) ve Yapay Arı Koloni (YAK) gibi bazı metasezgisel algoritmalar, PI kontrolör parametrelerinin optimal değerlerini elde etmede kullanılır. GKO algoritmasının kullanılan diğer algoritmalara göre

yakınsama hızı yavaş olmasına rağmen, en iyi dinamik performans GWO algoritmasıyla elde edilmiştir.

Anahtar Kelimeler: Üç Fazlı Asenkron Motor, Alan Yönlendirmeli Kontrol, Uvdgm, Matlab/ Simulink, Metasezgisel, PSO, Gko, Yak.

Bilim Kodu **:** 90514

ACKNOWLEDGMENT

I would like to express my deepest gratitude to my advisor, Dr. Hilmi AYGUN, whose sincerity and encouragement I will never forget. Dr. AYGUN has been an inspiration as I hurdled through the path of this Master's degree. He is the true definition of a leader and the ultimate role model. This thesis would not have been possible without Dr. AYGUN, whose guidance from the initial step of research enabled me to develop an understanding of the subject. I am thankful for the extraordinary experiences he arranged for me and for providing opportunities for me to grow professionally. It is an honor to learn from Dr. AYGUN.

I am grateful for my parents whose constant love and support keep me motivated and confident. My accomplishments and success are because they believed in me. My Deepest thanks to my friends, who keep me grounded, remind me of what is important in life, and are always supportive of my adventures.

CONTENTS

Page

APPROVAL ii
ABSTRACT iv
ÖZET vi
ACKNOWLEDGMENT viii
CONTENTS ix
LIST OF FIGURES xv
LIST OF TABLES xvi
SYMBOLS AND ABBREVIATIONS xvii

PART 1 1
INTRODUCTION 1
1.1. STATEMENT OF PROBLEM 1
1.2. AIM OF THE THESIS: 4
.1.3 OUTLINE OF THE THESIS 4

PART 2 6
LITERATURE SURVEY 6

PART 3 10
THEORETICAL BACKGROUND 10
3.1. BASIS OF INDUCTION MOTOR 10
3.2. TORQUE/ SPEED CURVE 13
.3.3 INDUCTION MOTOR MODEL 15
3.4. VECTOR CONTROL 17
3.5. SPACE VECTOR PULSE WIDTH MODULATION (SVPWM) 23

PART 4 30
METHODOLOGY 30
4.1. METAHEURISTIC OPTIMIZATION METHODS 30

Page

4.1.1. Particle Swarm Optimization (PSO) 31
4.1.2. Grey Wolf Optimization (GWO) 34
4.1.3. Artificial Bee Colony (ABC) 37

PART 5 40
SIMULATION RESULTS AND DISCUSSION 40
5.1. NO LOAD CONDITION 43
5.2. SPEED CHANGE CONDITION 45
5.3. SUDDEN LOAD CHANGE CONDITION 47

PART 6 51
CONCLUSION AND FUTURE WORK 51
6.1. CONCLUSION 51
6.2. FUTURE WORK 52

REFERENCES 53

RESUME 58

LIST OF FIGURES

Page

Figure 3.1. Cross sectional structure of squirrel cage IM 11
Figure 3.2. Torque - speed curve. 14
Figure 3.3. Block diagram of indirect Field Oriented Control (IFOC). 20
Figure 3.4. Clarke transformation vector. 21
Figure 3.5. Park transformation vector. 21
Figure 3.6. Inverse park transformation vector. 22
Figure 3.7. Inverse Clarke transformation vector. 23
Figure 3.8. Eight states for inverter ($V0\ to\ V7$). 24
Figure 3.9. Space vector diagram 25
Figure 3.10. Space vector of sector 1. 26
Figure 3.11. Switching by SVPWM method from sector 1 to sector 6 29
Figure 4.1. PSO flowchart. 33
Figure 4.2. Grey wolf social structure 34
Figure 4.3. GWO flowchart. 36
Figure 4.4. ABC Flowchart. 39
Figure 5.1. Speed at no load condition. 43
Figure 5.2. isd at no load condition. 44
Figure 5.3. isq at no load condition. 45
Figure 5.4. Speed at change condition. 46
Figure 5.5. isd at change condition. 46
Figure 5.6. isq at change condition. 47
Figure 5.7. Speed at sudden load condition. 48
Figure 5.8. isd at sudden load condition. 49
Figure 5.9. isq at sudden load condition. 49
Figure 5.10. Convergence speed of metaheuristic algorithms. 50

LIST OF TABLES

Page

Table 3.1. Relationship between switching vectors and voltages. 25
Table 3.2. Switching time for each sector. 28
Table 5.1. Induction motor parameters. 40
Table 5.2. PSO algorithm parameters. 41
Table 5.3. PSO- PI controller gains 42
Table 5.4. ABC algorithm parameters. 42
Table 5.5. ABC PI controller gains. 42
Table 5.6. GWO algorithm parameters. 42
Table 5.7. GWO PI controller gains 43
Table 5.8. Comparison between the responses of different algorithms at no load speed. 44

SYMBOLS AND ABBREVIATIONS

SYMBOLS

N_{syn}	:	Synchronous speed
V_s	:	Stator Voltage
w_g	:	General Angular Speed
f	:	Power Source Frequency
p	:	Number of Poles
s	:	Slip
N_{act}	:	Actual Speed
N_{slip}	:	Slip Speed
f^{-}	:	Frequency of Rotor
T	:	Torque
P_m	:	Mechanical Power
w_r	:	Rotor Speed
i_r	:	Rotor Current
w_{sl}	:	Slip Angular Speed
$IGBT_s$	:	Insulated Gate Bipolar Transistor
V_s	:	Stator Voltage
i_s	:	Stator Current
w_e	:	Speed in Synchronous Frame
L_s	:	Stator Inductance
L_r	:	Rotor Inductance
L_{ls}	:	Stator leakage Inductance
L_{lr}	:	Rotor leakage Inductance
i	:	Current Particle
i_r	:	Rotor Current
Ψ_s	:	Stator Flux

Ψ_r : Rotor Flux

i_d : Direct Axis Current

i_q : Quadrature Axis Current

V_d : Direct Axis Voltage

V_q : Quadrature Axis Voltage

Ψ_d : Direct Axis Flux

Ψ_q : Quadrature Axis Flux

P : Power

d : Number of Optimization Parameter

R_s : Stator Resistance.

R_r : Rotor Resistance

$\dot{\Psi}_s$: Reference Stator Flux.

$\dot{\Psi}_r$: Reference Rotor Flux

$\dot{w}_r$: Reference Rotor Speed

f_d : Friction Constant

T_L : Load Torque

n_p : Number of Pair Pole

T_e : Electromechanical Torque

M : Mutual Inductance

J : Inertia Torque

$\dot{\Psi}_d$: Reference Direct Axis Flux

$\dot{\Psi}_q$: Reference Quadrature Axis Flux

$\dot{i}_d$: Reference Direct Axis Current

$\dot{i}_q$: Reference Quadrature Axis Current

τ_r : Rotor Time Constant

σ : Leakage Factors

θ_r : Electrical Rotor Position

$\dot{\theta}_r$: Reference Electrical Rotor Position

K_t : Torque Constant

$\dot{T}_e$: Reference Torque

p : Local Best Position

g	:	Global Best Position
X_r	:	Reference Value
X_m	:	Measured Value
f_{cost}	:	Cost Function
w	:	Weighting Factor
α	:	Alpha
β	:	Beta
δ	:	Delta
ω	:	Omega
k	:	Randomly Integer Number Between [1, SN]
m	:	Number of Optimization Parameters
N	:	Element Number of X variable
i_a	:	a-Phase Current
i_b	:	b-Phase Current
i_c	:	c-Phase Current
i_α	:	Alpha Current
i_β	:	Beta Current
V_a	:	a-Phase Voltage
V_b	:	b-Phase Voltage
V_c	:	c-Phase Voltage.
V_{an}	:	Phase Voltage between a-Phase and Neutral
V_{bn}	:	Phase Voltage between b-Phase and Neutral
V_{cn}	:	Phase Voltage between c-Phase and Neutral
V_{ab}	:	Phase Voltage between a-Phase and b-Phase
V_{bc}	:	Phase Voltage between b-Phase and c-Phase
V_{ca}	:	Phase Voltage between c-Phase and a-Phase
V_α	:	Alpha Voltage
V_β	:	Beta Voltage
V_{ref}	:	Reference Voltage vector
$\overline{V_n}$	:	Better Fitness value
$\overline{X_p}$	:	Position Vector of Prey
f_s	:	Switching Frequency

$\bar{X}$	:	Position Vector of Grey Wolf
$\bar{a}$	:	Number Reduced From 2 to 0
θ_r	:	Rotational Frame Angle
θ_e	:	Synchronous Frame Angle
T_s	:	Switching Time
α	:	Angle Between Voltage Vectors
V_i^d	:	Velocity Factor of Factor (i) At Iteration (d)
C_1 **&** C_2	:	Acceleration Constant
r_1 **&** r_2	:	Random Number Between (0,1)
W	:	Iteration Factor.
t	:	Current Iteration
X	:	Position of Particle
X_1	:	Alpha Position
X_2	:	Beta Position
X_3	:	Delta Position
Q_{ni}	:	Random number
fit_n	:	Fitness Value of n solution
p_n	:	Probability of Selected Location
SN	:	Number of Food Sources

ABBREVIATIONS

IM	:	Induction Motor
AC	:	Alternating Current
DC	:	Direct Current
V/F	:	Constant Volts / Frequency
DE	:	Different Evolution Algorithm
FOC	:	Field Oriented Control
DTC	:	Direct Torque Control
VFD	:	Variable Frequency Drive
DFOC	:	Direct Field Oriented Control
IFOC	:	Indirect Field Oriented Control

SVPWM	:	Space Vector Pulse Width Modulation
GA	:	Genetic Algorithm
TLBO	:	Teacher Learner Based Optimization
DTC-SVM	:	Space Vector Modulation Direct Torque Control
GWO	:	Gray Wolf Optimization
PWM	:	Pulse Width Modulation
FOPI	:	Fractional Order Proportional Integral
ABC	:	Artificial Bee Colony
PID	:	Proportional Integral Derivative
QLSA	:	Quantum Behaved Search Algorithm
PI	:	Proportional Integral
PEO	:	Population Extremal Optimization
LSA	:	Lightening Search Algorithm
BSA	:	Backtracking Search Algorithm
GSA	:	Gravitation Search Algorithm
PSO	:	Particle Swarm Optimization
2-DOF	:	Two- Degree-of-Freedom
ACO	:	Ant Colony Optimization
ANFIS	:	Adaptive Network Based Fuzzy Interface Systems
ITAE	:	Integral Time Absolute Error
FLC	:	Fuzzy Logic Controller
DFIM	:	Doubly Fed Induction Motor
THD	:	Total Harmonic Distortion
MFs	:	Member Ship Functions
DSPs	:	Digital Signal Processors
d-q	:	Direct-Quadrature Axis Components
SAE	:	Sum of Absolute Error
SVM	:	Space Vector Modulation
CS	:	Cuckoo Search Algorithm
LTI	:	Linear Time Invariants

PART 1

INTRODUCTION

1.1. STATEMENT OF PROBLEM

Induction motors (IMs) become a part of daily life and they are used in household applications, industrial plants, laboratories, automation applications even in the field of electric vehicles. They have many advantages when compared to the other motors such as very simple structure, low cost, low maintenance, small volume, reliable torque response, high power density, high efficiency, robustness, and the ability to operate in difficult conditions [1].

IM consists essentially of two major parts called rotor and stator. The stator carries 3-phase windings which are placed in the slots with a phase difference of 120 degrees. Once the stator windings are fed from a 3-phase source, a rotating magnetic field is produced at synchronous speed in the stator. The magnetic field rotation leads to producing an electromotive force in the rotor. With the interaction of the rotor and stator magnetic fields, the rotor starts to rotate. However, there is a difference between the synchronous speed and rotor speed called the slip [2].

There are two types of IM because of different rotor structures:

- Squirrel-cage IM: Almost 90 % of the IMs are the squirrel-cage type because of their rugged and simple construction. The rotating part consists of a parallel slots and cylindrical core in which conductors are inserted. These conductors are not wires but consist of heavy bars of aluminum and copper. They are connected to the short circuit rings for the purpose of allowing a magnetic field to be generated in the rotor.

- Wound-rotor IM: In this type of IM, the windings in the rotor part are connected to external resistance through slip rings. Increasing the external resistance leads to improving starting torque. However, the value of this resistance must be zero to prevent the reduction of the efficiency of IM when the motor attains its full rated speed. However, wound-rotor IMs are more expensive; need more maintenance than squirrel-cage IMs. Also, they require complex automatic control circuit. Therefore, the usage of the wound-rotor IM is less than that of squirrel-cage IM [2] [3] [4].

The control of an IM is more difficult than that of a DC motor because of the nonlinear relationship between the stator current and flux or torque [5]. It remains a great challenging and complex problem for high-performance applications due to their nonlinearity parameters, and the rotor resistance thus the rotor time constant differs according to the operating conditions [6]. Therefore, various methods are proposed by researchers to improve the control of IM [7].

The control of IM has been improved in recent decades thanks to the development of microprocessors, microcontrollers, and power electronics. There are several significant control methods for IMs including:

- Voltage/frequency (V/ f) control (Scalar control)
- Field oriented control (FOC) (Vector control)
- Direct torque control (DTC)
- Space vector modulated- direct torque control (DTC-SVM).

The scalar control method aims to control the IM to operate in a steady state by varying the frequency and amplitude of the supply voltage at the same rate [8]. It is easy to implement and gives a superb steady-state response. However, it has a poor dynamic response due to the coupling effect of flux and torque since the torque and flux are functions of voltage and frequency respectively. As a result, it is used in low performance devices such as blowers, fans, and pumps [9].

High performance industrial applications such as robotics, rolling mills, and electric vehicles require fast and precise torque response with flux regulation. Several methods have been proposed to obtain these requirements. These methods are vector control or FOC, DTC, and DTC-SVM [10]. This thesis focuses on the FOC method.

FOC is the most suitable and popular control technique for three phase IMs at the lately. The essential principle of FOC is centered on the control of both the angle and the magnitude of each phase's voltage and current. The control implementation of FOC is based on vector conversions from the rotating frame to the stationary reference frame and the other way around.

A three-phase AC motor's stator currents are identified as two orthogonal components that may be represented by a vector in the FOC method which is a variable frequency drive (VFD) control technique. The orthogonal components are determined in a (*d*, *q*) coordinate system. The first representation of the stator current is the flux component which is aligned along the d (direct) axis and the second representation of the stator current is the torque component which is aligned along the q (quadrature) axis. Therefore, torque and flux are separated and controlled individually. Like a separately excited dc motor, the decoupling between torque and flux provides an excellent dynamic response for IM. As a result, FOC based IM drives are used widely in high performance applications, where high precision and a wide range of variable speed control are needed [1] [10] [11] [12].

In FOC, voltage and current sensors are usually used, and speed sensor may be needed to increase system performance. Its practical application is realized by integrated digital circuits, such as digital signal processors (DSPs), microcontrollers and microcomputers [13].

The FOC can be divided into two types, ‘‘Direct Field Oriented Control’’ (DFOC) and ‘‘Indirect Field Oriented Control’’ (IFOC) [9]. The space vector pulse width modulation (SVPWM) is utilized in both FOC methods to control the essential components of the stator current [14]. FOC method consists of three PI controllers used in speed, torque, and flux control. Tuning PI controller parameters is a

challenging problem. Most of the time, these parameters are determined by trial and error. Sometimes, they are chosen by the Ziegler Nichols method due to the step response. However, these methods cause a poor dynamic response under variable speed reference and sudden load change.

1.2. AIM OF THE THESIS:

The aims of this thesis are listed below:

- To create a model of FOC based IM drive system using MATLAB.
- To develop PI controllers used in speed, flux and torque control of IM based on FOC using some metaheuristic strategies like particle swarm optimization (PSO), grey wolf optimization (GWO) and artificial bee colony (ABC) algorithm.
- To determine the best optimization method for high precision speed control, accurate and fast response of the torque and flux at variable speeds and loads.

1.3. OUTLINE OF THE THESIS

In this thesis, controller design based on metaheuristic methods will be developed and these controllers will be applied to the FOC based IM drive.

In Chapter 2, the review of studies about FOC based IM is presented, and then a review of studies on controller design based on metaheuristic methods is also presented.

In Chapter 3, the mathematical model of IM is given and description of proposed control method by using FOC based IM is also presented.

In Chapter 4, the description of the proposed metaheuristic optimization methods for the PI controllers using FOC of IM is presented.

In Chapter 5, simulation results are given, and the performance of the PI controllers is compared. According to the comparison, the best metaheuristic method is determined for FOC based IM drives.

Chapter 6 concludes all work carried out and suggests some points which need to be improved for future works.

PART 2

LITERATURE SURVEY

In the recent studies, rather than obtaining linear models for every control loop of IM, metaheuristic optimization algorithms have been used as alternative methods for optimizing controller parameters with non-linear model of IM. In [15], PSO method was used to obtain the optimum parameters of PI and PID controllers for the speed control of FOC based IM. Simulation results were compared with the traditional Ziegler-Nichols method. They showed that PSO was more efficient in improving the step response for controlling the speed. Also, the PSO method provided more stable results, and computational efficiency.

In [16], Ant Colony Optimization (ACO) algorithm was utilized in the vector control of IM. This study presented a complex method of online optimization and online identification of the controller parameters to obtain steady state accuracy and better dynamic performance during operation such as changes in frequency, magnetic field, temperature, and other factors which cause changes in mechanical and electrical parameters of IM. The simulation results showed improvement in steady state characteristics and dynamic performance.

In [17], a vector-controlled IM drive was designed to improve efficiency and to reduce torque fluctuations. PSO algorithm was used to resolve issues with nonlinear optimization and find the best solutions. In two cases, parameters of PI controller were optimized. In the first case, the parameters were calculated to improve overall system efficiency, while in the second situation, the parameters were calculated to both improve efficiency and reduce torque fluctuations. The results showed that torque fluctuations in the steady state were significantly reduced when torque fluctuations were taken into account for the objective function. Consequently, less stator current and DC link voltage fluctuations were obtained.

[18] utilized neural network for tracking the reference speed of an indirect FOC based IM. The authors concluded that utilizing a neural network for speed control is more useful, more successful, and capable of enhancing performance and reducing the ripple when compared with a traditional PI controller.

In [19], a prototype model was developed by employing the PSO-ANFIS hybrid approach to control the speed of an IM. Two characteristics were employed as inputs: speed and torque, and the output were the firing angle. Optimal dynamic behavior and greater speed control performance of the IM were obtained by the PSO-ANFIS speed controller. In this study, a comparison analysis was carried out between fuzzy back propagation and the PSO-ANFIS algorithm, while the PSO-ANFIS performed superior in terms of fast computation.

In [20], a backtracking search algorithm (BSA) based adaptive fuzzy logic controller (FLC) was designed for speed control an IM drive. This technique was used to alter the membership functions (MFs) automatically for FLC. To avoid the traditional way of obtaining the optimal MFs by trial and error, the created BSA based FLC was employed. IM drive was modeled by using the SVPWM approach with V/f control. To confirm the activity of the BSA based FLC controller, the responses of BSA based FLC, gravitational search algorithm (GSA) based FLC, and PSO based FLC were compared. The obtained results demonstrated that the BSA based FLC controller is superior to the GSA based FLC and PSO based FLC controllers in terms of damping ability, robustness, and improvement of the transient responses of IM. Additionally, the BSA based FLC controller provided considerable decreases in speed response in terms of settling time, steady-state error, and overshoot.

In [21], quantum behaved lightening search algorithm (QLSA) for the purpose of designing a fuzzy based PI controller was applied to indirect FOC (IFOC) based IM drive. The results showed that the QLSA based IFOC is more efficient than the lightening search algorithm (LSA) based IFOC, BSA based IFOC, PSO based IFOC and GSA based IFOC in terms of damping capability, robustness, and improvement in transient responses.

In [22], Ant Colony Optimization (ACO) and Differential Evolution (DE) algorithms were applied to enhance the PI controller parameters in the case of DTC-SVM based IM control loops, like torque, speed, stator flux linkage and evaluation of stator flux linkage. The results showed that the DTC-SVM architecture using optimized PI controllers performed well. The performance of DE algorithm optimization method was slightly better than ACO when considering both speed reversion and load disturbance tests.

In [23], genetic algorithm (GA) was applied to solve equations of d-q model of the IM. To get successful results, GA used two types of chromosomes encoding, including binary and floating, as well as some crossover, mutation, and selection. Using floating point encoding in simulations gave better results than binary encoding. The usage of GA eliminated the overshoot in speed response of IM.

In [24], a combination of Kharitonov's theorem and PSO in a single optimization process was presented as the best IM control design solution against parameters uncertainty. The method was applied for designing the FOC-based PI controllers for an IM. In contrast to earlier studies, which were applied to determine the objective function of either the frequency or time domains, this approach relied on evaluating the behavior of the system in both the frequency and time domains. A high level of stability against parameter uncertainty was provided by the developed controller. An effective optimization process was produced by excluding weak particles that provide undesirable frequency or time responses and may also violate the stability constraints.

In [25], a comparison study using PSO, JAYA algorithm and Teacher Learner based Optimization (TLBO) algorithm was presented for tuning Fractional-order PI (FOPI) and PI controllers to obtain the optimal controller parameters in indirect vector-controlled IM. The results showed that JAYA algorithm provided a better response in steady state than the other strategies.

In [26], population extremal optimization (PEO) algorithm was used to optimize PID controller of speed control loop which had a two-degree-of-freedom (2-DOF)

structure to smooth the electromagnetic torque responses without adjusting the current controllers in FOC based IM. As the goal function for controller optimization, the integral time absolute error (ITAE) and a chattering penalty function were used. The goal function value of the PEO-based 2-DOF control was lower than that of designs based on GA and PSO.

In [27], ACO algorithm was used to optimize PID speed controller of DTC based doubly fed induction motor (DFIM). This study confirmed several improvements in the controller performance, such as flux and torque ripples, speed overshoot, and total harmonic distortion (THD) of currents which are major factors for the DTC robustness. It was validated experimentally on dSPACE Board DS1104.

PART 3

THEORETICAL BACKGROUND

3.1. BASIS OF INDUCTION MOTOR

In this section, the theoretical aspect of a three-phase IM squirrel cage type is presented. The rotor part of the squirrel cage IM consists of heavy bars of aluminum, copper and brass which create a short circuit and the rotor generates the magnetic field and induction current by itself, this is the reason which makes the IM is a rugged, robust, and cheap candidate for motor drive systems [3] [28]. Figure 3.1 shows the cross-sectional structure of the squirrel cage IM. Three phase AC voltages are fed to the three phase stator terminals and the currents flowing produce a rotating magnetic field through the stator windings. The rotation the magnetic field speed is defined as synchronous speed which depends on the source's frequency and the poles number [29].

$$N_{syn} = \frac{120\ f}{p} \tag{3.1}$$

Where N_{syn} is the synchronous speed, f is the power source frequency, p is the poles number.

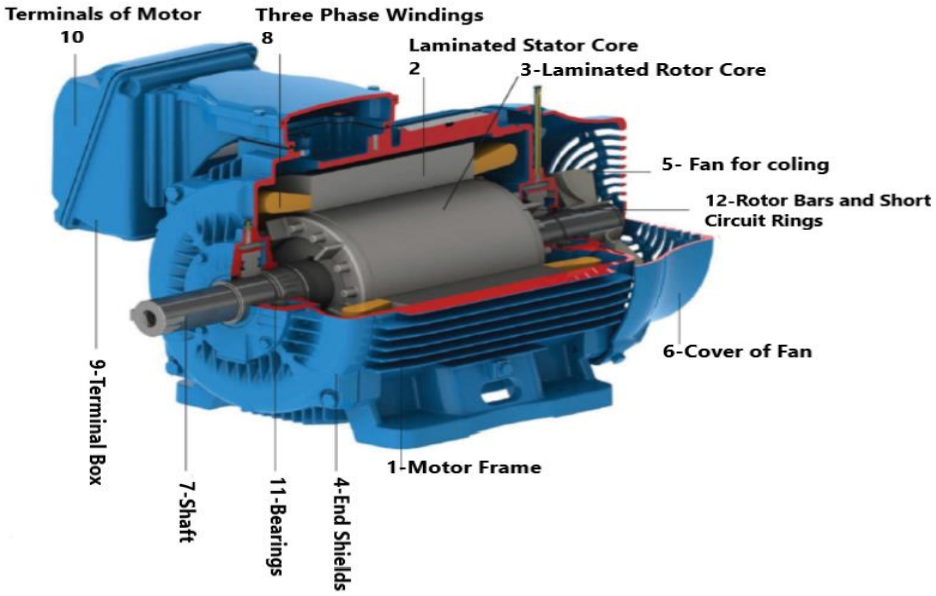

Figure 3.1.Cross sectional structure of squirrel cage IM [30].

The rotating magnetic field which is produced on the stator will cause a voltage to be induced in the rotor bars. The circulating electric current is generated in the rotor bars due to the short circuit of the rotor bars and it causes the induced rotor electric current interacts with the rotating magnetic field. A tangential electromagnetic force is created on the rotor bars according to Lorentz's law, in which by adding all the forces on every rotor bar, a torque is produced and finally, the rotor is driven in the rotating field direction [31].

At the beginning of the generation of the rotating magnetic field, the rotor remains at the break condition. Then the rotor starts to accelerate quickly to reach the rotating stator flux; with increasing speed, the rotor bars do not cut the same amount as the rotating field, therefore the rotor bars' voltage decreases. When the rotor speed is equal to the synchronous speed, the rotor bars do not cut the field then the rotor begins to decelerate. For this reason, IMs are called asynchronous motors because the rotor speed is different from the synchronous speed [30].

The slip may be defined as the difference between the synchronous speed N_{syn} and actual speed N_{act} of the rotor; it can be expressed as a percentage of the synchronous speed.

$$\% \text{ slip } \% s = \frac{N_{syn} - N_{act}}{N_{syn}} \times 100 \quad (3.2)$$

Usually, $N_{syn} - N_{act}$ is called the slip speed.

$$N_{slip} = N_{syn} - N_{act} \quad (3.3)$$

$$\% s = \frac{N_{slip}}{N_{syn}} \times 100 \quad (3.4)$$

The rotor (or actual) speed is:

$$N_{act} = N_{syn}(1 - s) \quad (3.5)$$

Where s is slip, N_{syn} is synchronous speed, N_{act} is actual speed and N_{slip} is slip speed.

If the rotor speed and synchronous speed are equal, then s=0, but if the rotor speed is equal to zero, then s=1. Slip speed is defined below due to the rotor frequency (f'):

$$N_{syn} - N_{act} = \frac{120f'}{p} \quad (3.6)$$

By dividing eq. (3.6) by eq. (3.1), we obtain:

$$\frac{f'}{f} = \frac{N_{syn} - N_{act}}{N_{syn}} = s \quad (3.7)$$

$$f' = sf \quad (3.8)$$

By substituting the two equations (3.1 & 3.2) into equation 3.8. [2] [32], we obtain:

$$f' = \frac{p}{120}\left(N_{syn} - N_{act}\right) \tag{3.9}$$

3.2. TORQUE/ SPEED CURVE

The calculation of the rotor current is necessary to obtain the torque of IM. The torque of an IM is given by:

$$T = \frac{P_m}{\omega_r} = 3|i_r^2|\frac{(1-s)R_r}{s\omega_r} \tag{3.10}$$

The rotor current of IM is calculated by:

$$|i_r| = \frac{|v_S|}{\sqrt{\left(R_s + \frac{R_r}{s}\right)^2 + \omega_e^2(L_{ls} + L_{lr})^2}} \tag{3.11}$$

Where T is torque, P_m is mechanical power, ω_r is rotor speed, i_r is rotor current, R_r is rotor resistance, R_s is stator resistance, v_s is stator voltage, ω_e is speed in synchronous frame, L_{ls} is stator leakage inductance, L_{lr} is rotor leakage inductance.

$\frac{1-s}{\omega_r}$ From slip equations, we get that $\frac{P}{2\omega_e}$ =

The electromagnetic torque can be calculated by:

$$T_e = \frac{3\ P\ R_r}{2\ s\ \omega_e}\frac{|v_S|^2}{(R_s + \frac{R_r}{s})^2 + \omega_e^2(L_{ls} + L_{lr})^2} \tag{3.12}$$

If the slip is very small $(s \approx 0)$, the approximate equation for torque is as follows:

$$T_e \cong \frac{3\ P\ R_r}{2\ s\ \omega_e}\frac{|v_S|^2}{\left(\frac{R_r}{s}\right)^2} \cong \frac{3P\ s}{2\ \omega_e}\frac{|v_S|^2}{R_r} \tag{3.13}$$

In the small slip area, the torque curve is in the form of a straight line near s=0, but if s=1, the approximate equation for torque is as follows:

$$T_e = \frac{3\ P\ R_r}{2\ s\ \omega_e} \frac{|v_S|^2}{(R_s + R_r)^2 + \omega_e^2 (L_{ls} + L_{lr})^2} \tag{3.14}$$

Where P is power, T_e is electromagnetic torque [33].

The torque of 3-phase IMs depends on the speed; and the relationship between them is complex and can't be expressed by a simple equation, so it is easy to express this relation in the form of the curve as shown below in the Figure (3.2).

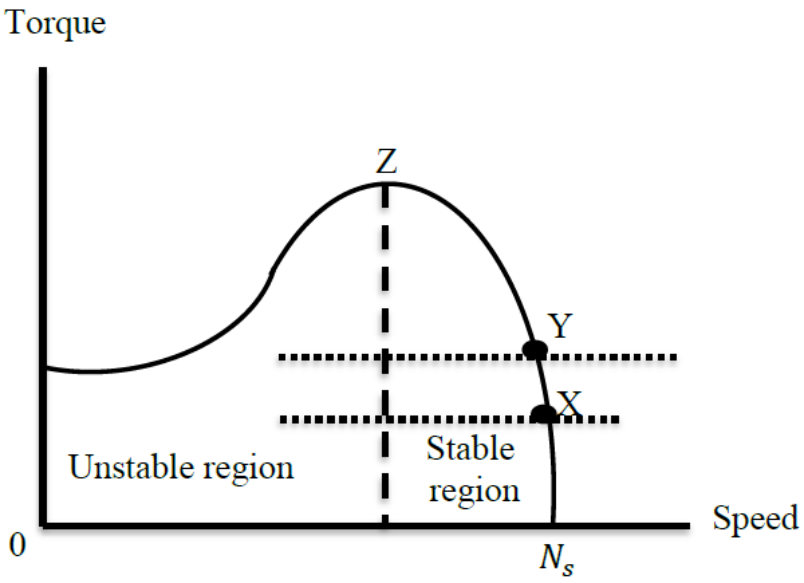

Figure 3.2. Torque - speed curve.

In this curve, when the speed is zero (N=0), the starting torque is approximately equal to 1.5 T and it is called locked rotor torque. But at the point Z, while the speed reaches about 80 % of the synchronous speed N_{syn}, the torque value becomes maximum (2.5 T) and it is called the breakdown torque. The point X represents the full load torque (T) at a given actual speed (N). With increasing the mechanical load, the motor speed decreases until the motor torque becomes equal to the load torque. Then, the motor will run slowly at a constant speed. If the load torque exceeds the point Z, the motor stops working suddenly [34].

3.3. INDUCTION MOTOR MODEL

There are several ways for modelling IM. The state variable form is more useful for expressing the IM mathematical model, so it will be used in this thesis. A fifth-order model with speed and four electrical state variables can be used. [35]. By adding position (angle) variable, the sixth-order model can be used too. Different choices for modelling are available including the electrical state variables such as stator and rotor currents or stator, rotor, and airgap flux variables. These two-dimensional variables have direct (d) and quadrature (q) axis components. Furthermore, there are different choices for the determination of the reference frame such as stationary or synchronously rotating reference frames. A general reference frame that rotates at a general angular speed ω_g can be selected. When the general angular speed ω_g is equal to zero, the stationary reference frame is obtained. When the general angular speed ω_g and synchronous speed are equal, the synchronously rotating reference frame is obtained. In this thesis, the model is given in general reference frame. The state variables such as stator current i_s, rotor flux Ψ_r, rotor electrical angular speed ω_r, and the inputs such as stator voltage v_s are given in the following equations [35].

$$i_s = i_d + j i_q \tag{3.15}$$

$$\Psi_r = \Psi_d + j\Psi_q \tag{3.16}$$

$$v_s = v_d + j v_q \tag{3.17}$$

$$v_s = R_s i_s + j\omega_g \Psi_s + \dot{\Psi}_s \tag{3.18}$$

$$0 = R_r i_r + j(\omega_g - \omega_r)\Psi_r + \dot{\Psi}_r \tag{3.19}$$

$$T_e = \frac{3}{4} p(\Psi_s \times i_s) = J\,\dot{\omega}_r + f_d \omega_r + T_L \tag{3.20}$$

Where J is inertia torque, T_L and T_e are load and electromagnetic torque respectively, f_d is friction constant. The stator flux Ψ_s and rotor flux Ψ_r can be expressed by the following equations.

$$\Psi_s = L_s i_s + M i_r \tag{3.21}$$

$$\Psi_r = L_r i_r + M i_s \tag{3.22}$$

Where L_s , L_r and M are stator, rotor, and mutual inductance respectively. The 5th order model of IM in state variable form can be expressed as:

$$\dot{i}_d = -\frac{L_r R_s + {M^2}/{\tau_r}}{\sigma L_s L_r} i_d + \omega_g i_q + \frac{M}{\tau_r \sigma L_s L_r} \Psi_d + \frac{M}{\sigma L_s L_r} \omega_r \Psi_q + \frac{1}{\sigma L_s} v_d \tag{3.23}$$

$$\dot{i}_q = -\frac{L_r R_s + {M^2}/{\tau_r}}{\sigma L_s L_r} i_q - \omega_g i_d + \frac{M}{\tau_r \sigma L_s L_r} \Psi_q - \frac{M}{\sigma L_s L_r} \omega_r \Psi_d + \frac{1}{\sigma L_s} v_q \tag{3.24}$$

$$\dot{\Psi}_d = \frac{M}{\tau_r} i_d - \frac{1}{\tau_r} \Psi_d + (\omega_g - \omega_r) \Psi_q \tag{3.25}$$

$$\dot{\Psi}_q = \frac{M}{\tau_r} i_q - \frac{1}{\tau_r} \Psi_q - (\omega_g - \omega_r) \Psi_d \tag{3.26}$$

$$\dot{\omega}_r = \frac{3}{2} \frac{n_p M}{J L_r} (\Psi_d i_q - \Psi_q i_d) - \frac{f_d}{J} \omega_r - \frac{1}{J} T_L \tag{3.27}$$

Where $\sigma = (L_r L_s - M^2)/(L_s L_r)$ is the leakage constant and $\tau_r = L_r/R_r$ is rotor time constant. The electrical dynamics are expressed by equations (3.23)-(3.26), whereas the mechanical dynamic is expressed by Equation (3.27). Occasionally, the electrical rotor position θ_r is considered as the sixth state variable.

$$\dot{\theta}_r = \omega_r \tag{3.28}$$

In this modelling, the saturation of flux, iron losses and harmonics are ignored, and the IM is assumed to be operating in a balanced condition [35].

3.4. VECTOR CONTROL

Vector control, which also called field-oriented control (FOC), is one of the types of variable frequency drive (VFD) control method. In this method, the stator currents of a 3-phase electric motor are represented by two - orthogonal components (*d*-*q*) in the form of a vector. While *q*-component axis current controls the torque, and *d*-component axis current controls the magnetic flux. The control system computes the corresponding references of current components from the torque and flux references. While the torque reference value is obtained by the speed controller, the flux reference value is determined by the user. FOC method is generally used to control AC induction and synchronous motors. It was proposed for high performance applications that require operating well at the full load, high dynamic performance in terms of acceleration and deceleration, generation full load torque at zero speed [36]. Vector control operation of IMs is analogous to the operation of the separately excited DC motors. In the separately excited DC - motors, the field flux linkage and armature flux linkage created by the armature and respective field currents are orthogonally aligned. The field flux linkage doesn't change when the torque is controlled and therefore a high dynamic torque response is obtained. In the FOC of induction motor, the space vector of a complex stator current can be expressed in a coordinate system with orthogonal components along *d*-*q* axes. The field flux linkage component is aligned with the *d*-axis, but the torque component is aligned with the-*q* axis [37].

Vector control results in smoother transient response and steady-state response. It can be divided into two main categories: the direct field-oriented control (DFOC) and the indirect field field-oriented control (IFOC). The rotor angle is determined differently in the two approaches. [38]. To conduct the frame transformation in FOC, a precise rotor flux position must be obtained. The information of the rotor angle is critical in vector control. The rotor angle is sensed using Hall sensors or estimated using an adaptive approach. The performance of the IFOC and DFOC of an IM that

is fed with a multi-level inverter in low and high-speed operation is analyzed. The IFOC is appropriate for low-speed operation, whereas the DFOC is appropriate for rated-speed operation. Vector control requires knowledge of IM parameters, coordinate transformation, current controllers. It allows for a wide range of speed control. It requires instantaneous control of the angle and magnitude of the space vector [39]. The electromagnetic torque can be expressed by substituting the equations (3.21) & (3.22) in equation (3.20).

$$T_e = \frac{3}{2} n_p \frac{M}{L_r} (\Psi_r \times i_s) = \frac{3}{2} n_p \frac{M}{L_r} \left(\Psi_d i_q - \Psi_q i_d \right) \tag{3.29}$$

To simplify electromagnetic torque expression, the direct axis of the reference frame is locked onto the rotor flux vector, so $\Psi_q = 0$. Then general angular speed ω_g and synchronous angular frequency ω_s become similar and the equation of the torque becomes the same as that of the DC motors. Also, electrical variables become slowly varying like those of DC motors.

In FOC, the angle between the stationary and rotating reference frames must be found in order to convert the variables between these reference frames. This can be done by using two ways. The first way is Direct Field-Oriented Control (DFOC). In this way, the angle of the flux vector in the stationary reference frame is taken as the angle of the *d* axis of the rotating reference frame. As a result, Ψ_q and $\dot{\Psi}_q$ become equal to zero. Then the slip angular frequency (ω_{sl}) can be found from the Equation (3.26).

$$\omega_{sl} = \omega_s - \omega_r = \frac{M i_q}{\tau_r \Psi_d} \tag{3.30}$$

The second way is Indirect Field Oriented Control (IFOC). In this way, the slip frequency is taken as in equation (3.30). If equation (3.30) is substituted into equation (3.26), then equation (3.31) is obtained.

$$\dot{\Psi}_q = -\frac{1}{\tau_r}\Psi_q \tag{3.31}$$

If the magnetizing current component, i_d, is maintained constant at its reference value i_d^*, and $\Psi_q = 0$ is substituted into Equation (3.25), Equation (3.32) is obtained.

$$\Psi_d = \Psi_d^* = Mi_d = Mi_d^* \tag{3.32}$$

Where Ψ_d^* is a constant reference value for the magnitude of rotor flux at the equilibrium. Then the magnetizing current reference is determined as:

$$i_d^* = \frac{\Psi_d^*}{M} \tag{3.33}$$

By substituting equation (3.32) in to equation (3.30), the slip frequency command is determined as:

$$\omega_{sl} = \omega_s - \omega_r = \frac{i_q}{\tau_r i_d^*} \tag{3.34}$$

The equation of the electromagnetic torque (3.29) becomes proportional to i_q

$$T_e = K_t i_q \tag{3.35}$$

Where K_t is the torque constant, and it is given by:

$$K_t = \frac{3n_p M^2 i_d^*}{2L_r} \tag{3.36}$$

Therefore, i_q is the current component or sometimes called the torque current that produces the torque. In the control of speed, the torque demand T_e^* is the output signal of the Proportional-Integral (PI) speed controller, of which feeding is the error

between the reference speed ω_r^* and feedback speed ω_r. For the control of torque, the torque current reference i_q^* is determined by [35]:

$$i_q^* = \frac{T_e^*}{K_t} \tag{3.37}$$

IFOC method will be used in this thesis to control for three-phase IM. The IFOC system has two inputs: the speed and the torque reference command, and the rotor reference flux. An IFOC system for an IM allows decoupling control of the flux and torque. Figure 3.3 depicts a general block diagram of an IFOC system for an IM [40].

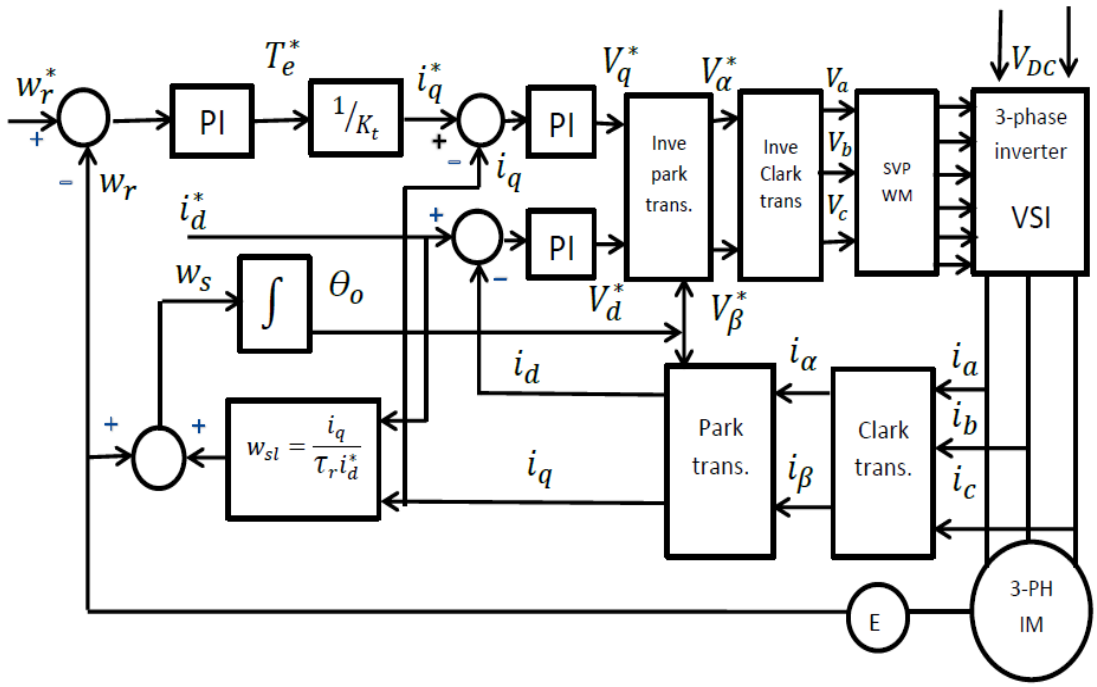

Figure 3.3. Block diagram of indirect Field Oriented Control (IFOC).

The main steps required for IFOC are summarized as follows:

Step 1: The rotor speed ω_r and 3-phase stator currents i_a , i_b, and i_c are measured.
Step 2: The 3-phase stator currents are converted into two-axis currents i_α and i_β by using a Clarke transformer as shown below in figure 3.4.

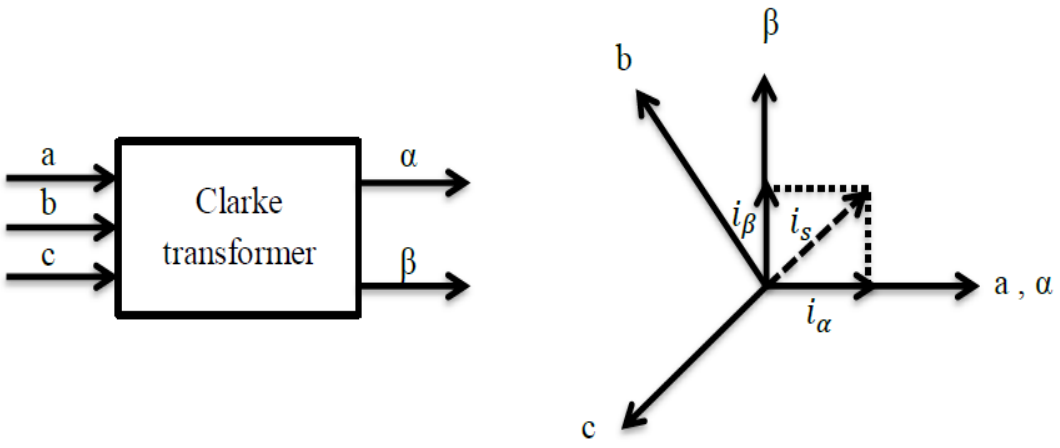

Figure 3.4.Clarke transformation vector.

The equations for Clarke transformation are written below:

$$i_a + i_b + i_c = 0 \tag{3.38}$$

$$i_\alpha = i_a \tag{3.39}$$

$$i_\beta = \frac{i_a + 2i_b}{\sqrt{3}} \tag{3.40}$$

Step 3: The two-axis currents i_α and i_β are transformed to other two-axis currents i_d and i_q by using a park transformer as shown in figure 3.5. Thanks to the park transformation, two-coordinate linear time invariant (LTI) system is obtained. Thus, LTI system lets the use of simple and easy to apply PI controllers and simplifies the control of torque and flux producing currents.

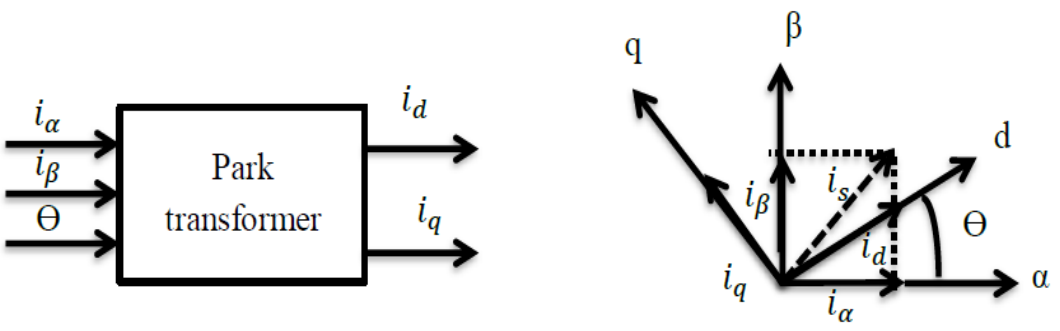

Figure 3.5. Park transformation vector.

The equations for park transformation are written below:

$$i_d = i_\alpha \cos\theta + i_\beta \sin\theta \tag{3.41}$$

$$i_q = -i_\alpha \cos\theta + i_\beta \sin\theta \tag{3.42}$$

Step 4: The i_d reference is employed to control the rotor magnetizing flux. The i_q reference is employed to control the torque. The errors are calculated by comparing i_d, i_q, and their reference values. The errors are given as inputs of PI controllers and V_d and V_q which are the voltage vector components, are obtained for feeding the IM.

Step 5: the PI controllers' output values (V_d and V_q) are transformed into the stationary reference frame by an inverse park transformer as shown in figure 3.6 Thus, V_α and V_β voltage values are obtained.

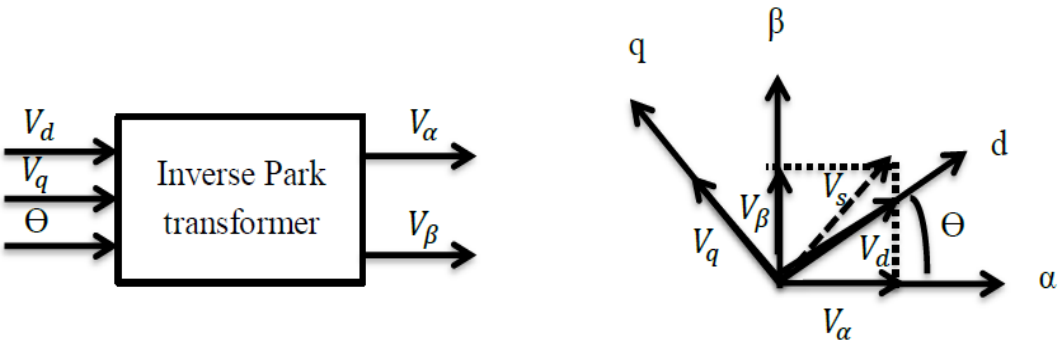

Figure 3.6. Inverse park transformation vector.

The equations for inverse-park transformation are given below:

$$V_\alpha = V_d \cos\theta - V_q \sin\theta \tag{3.43}$$

$$V_\beta = V_d \sin\theta + V_q \cos\theta \tag{3.44}$$

Step 6: The values (V_α and V_β) are transformed to three-phase voltage values by using an inverse-Clarke transformer as shown in figure 3.7 and used to calculate SVPWM duty cycle values.

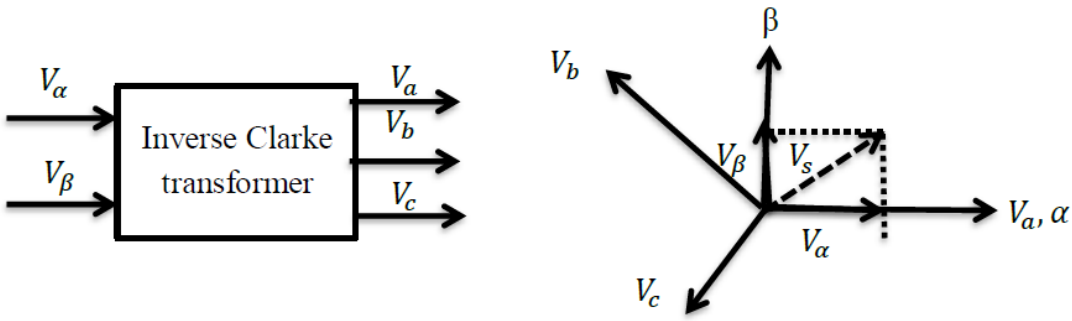

Figure 3.7. Inverse Clarke transformation vector.

The equations for inverse-Clarke transformation are given below [40]:

$$V_a = V_\beta \tag{3.45}$$

$$V_b = \frac{V_\beta + \sqrt{3}\, V_\alpha}{2} \tag{3.46}$$

$$V_c = \frac{V_\beta + \sqrt{3}\, V_\alpha}{2} \tag{3.47}$$

3.5. SPACE VECTOR PULSE WIDTH MODULATION (SVPWM)

Space Vector Modulation (SVM) method generates PWM control signals in a three-phase inverter, and it has been proven to be the best methodology for VFD applications. In comparison to other PWM techniques, this approach has a better strategy for achieving a high output voltage, minimizing harmonic output, and reducing switching losses. The IGBTs used as switches in the inverter circuit are shown in Figure 3.8. The upper IGBTs (S1, S3, and S5) are equal to 1 when the switch is ON, but the lower IGBTs (S2, S4, and S6) are equal to 0 when the switch is OFF. The output voltage may be calculated using the ON and OFF cases of the upper IGBTs. The line-to-line voltages (V_{ab}, V_{bc}, and V_{ca}) can be written by the following equation.

$$\begin{bmatrix} V_{ab} \\ V_{bc} \\ V_{ca} \end{bmatrix} = V_{dc} \begin{bmatrix} 1 & -1 & 0 \\ 0 & 1 & -1 \\ -1 & 0 & 1 \end{bmatrix} \begin{bmatrix} S_1 \\ S_3 \\ S_5 \end{bmatrix} \quad (3.48)$$

But the line-to-neutral voltages (V_{an}, V_{bn}, and V_{cn}) can be expressed by the following equation [41] [42].

$$\begin{bmatrix} V_{an} \\ V_{bn} \\ V_{cn} \end{bmatrix} = \frac{V_{dc}}{3} \begin{bmatrix} 2 & -1 & -1 \\ -1 & 2 & -1 \\ -1 & -1 & 2 \end{bmatrix} \begin{bmatrix} S_1 \\ S_3 \\ S_5 \end{bmatrix} \quad (3.49)$$

Due to the switching partners, eight switching vectors are obtained in the three-phase inverter. Two of them are zero vectors (V0, V7), and the other six vectors are non-zero vectors (V1, V2, V6). It means that if the zero vectors are used in the inverter, the currents of IM will be zero.

Figure (3.8) and Table 3.1 illustrate the eight-switching vectors, output line-to-neutral voltages, and output line-to-line voltages.

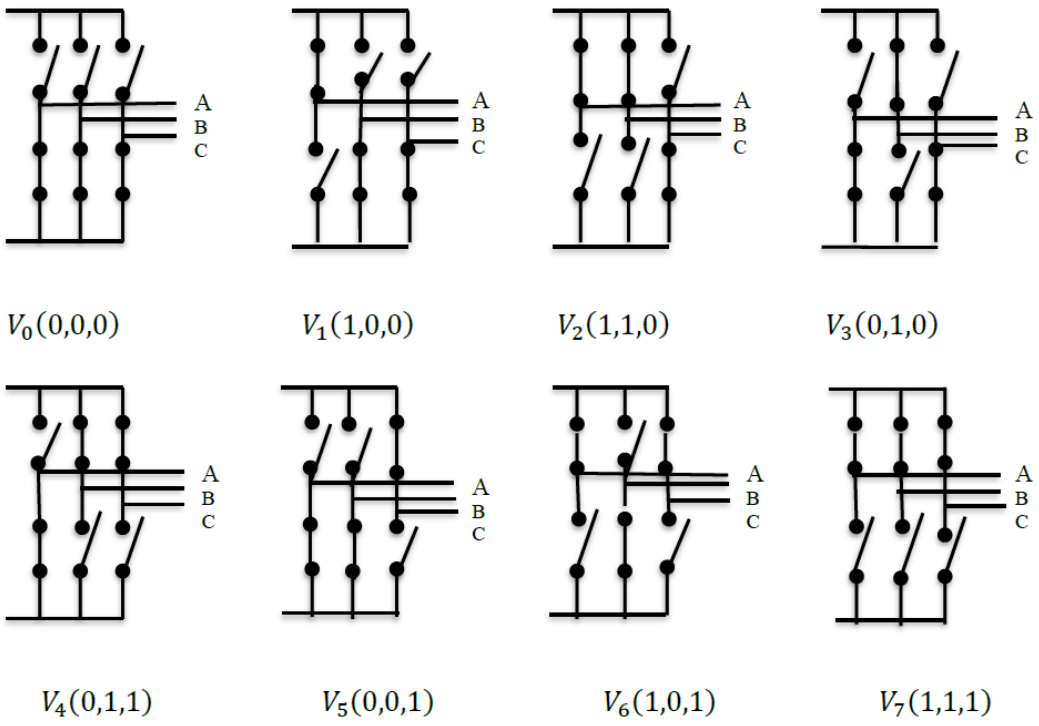

Figure 3.8. Eight states for inverter (V_0 *to* V_7).

Table 3.1. Relationship between switching vectors and voltages.

Voltage vectors	Switching vectors			Line to neutral voltage			Line to Line voltage		
	S_1	S_3	S_5	V_{an}	V_{bn}	V_{cn}	V_{ab}	V_{bc}	V_{ca}
V_0	0	0	0	0	0	0	0	0	0
V_1	1	0	0	$2/3V_{dc}$	$-1/3V_{dc}$	$-1/3V_{dc}$	V_{dc}	0	$-V_{dc}$
V_2	1	1	0	$1/3V_{dc}$	$1/3V_{dc}$	$-2/3V_{dc}$	0	V_{dc}	$-V_{dc}$
V_3	0	1	0	$-1/3V_{dc}$	$2/3V_{dc}$	$-1/3V_{dc}$	$-V_{dc}$	V_{dc}	0
V_4	0	1	1	$-2/3V_{dc}$	$1/3V_{dc}$	$1/3V_{dc}$	$-V_{dc}$	0	V_{dc}
V_5	0	0	1	$-1/3V_{dc}$	$-1/3V_{dc}$	$2/3V_{dc}$	0	$-V_{dc}$	V_{dc}
V_6	1	0	1	$1/3V_{dc}$	$-2/3V_{dc}$	$1/3V_{dc}$	V_{dc}	$-V_{dc}$	0
V_7	1	1	1	0	0	0	0	0	0

The switching vectors and sectors are shown in Figure 3.9. There are 60 degrees between the sectors. As an example, the reference voltage vector is in sector 1 due to the Figure 3.9.

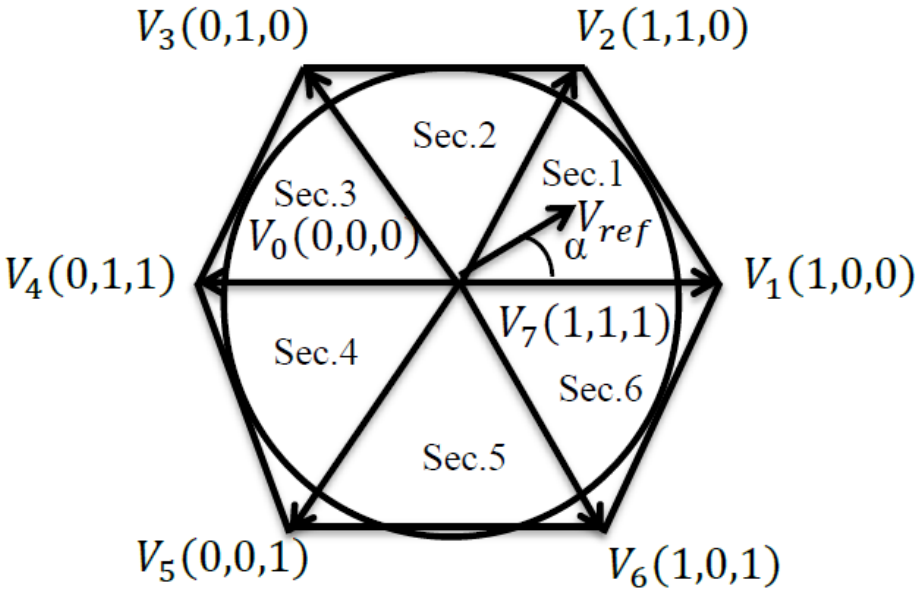

Figure 3.9. Space vector diagram [43].

The V_α and V_β voltages are utilized to calculate the magnitude of the reference voltage vector (V_{ref}) and the angle (α) between the voltage vectors in the hexagon. These values can be determined as follows.

$$|V_{ref}| = \sqrt{V_\alpha^2 + V_\beta^2} \tag{3.50}$$

$$\alpha = tan^{-1}\frac{V_\beta}{V_\alpha} \tag{3.51}$$

For example, if V_{ref} is in sector 1 as shown in Figure 3.10, it can be synthesized by the vectors in that sector as follows.

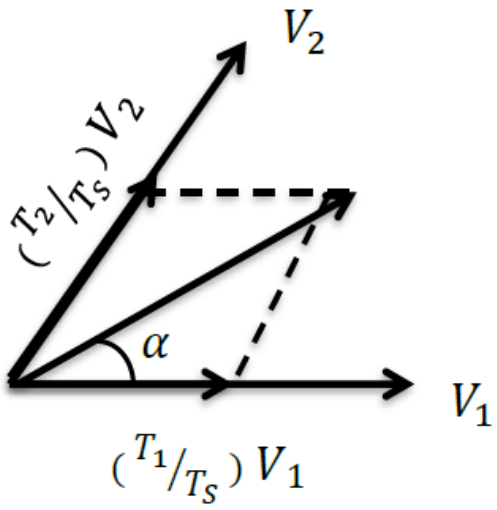

Figure 3.10. Space vector of sector 1.

In a sampling time T_s given by Equation 3.53, the corresponding space vector in sector 1 is applied by the non-zero vectors $\bar{V}_1$ and $\bar{V}_2$ during the T_1 and T_2 time durations, and the zero vector $\bar{V}_0$ during the T_0 time duration as given in Equation 3.52.

$$\int_0^{T_s} \bar{V}_{ref}\,dt = \int_0^{T_1} \bar{V}_1 dt + \int_{T_1}^{T_1+T_2} \bar{V}_2 dt + \int_{T_1+T_2}^{T_s} \bar{V}_0 dt \tag{3.52}$$

$$T_s = \frac{1}{f_s} \tag{3.53}$$

Where T_s is the switching time, and f_s is the switching frequency.

The time duration of switching vectors in each sector (n) may be determined by the following equations.

$$T_1 = \frac{\sqrt{3}.T_s.|V_{ref}|}{V_{dc}} \sin\left(\frac{n}{3}\pi - \alpha\right) \tag{3.54}$$

$$T_2 = \frac{\sqrt{3}.T_s.|V_{ref}|}{V_{dc}} \sin(\alpha - \frac{n-1}{3}\pi) \tag{3.55}$$

$$T_0 = T_s - (T_1 + T_2) \tag{3.56}$$

Thanks to the SVPWM method, a constant switching frequency is provided as seen in Figure 3.11 and thus, the switching losses are reduced. Table 3.2 shows the switching time for six switches in any sector [44].

Table 3.2. Switching time for each sector.

Sector	Upper switching	Lower switching
1	$T_a = T_1 + T_2 + \frac{T_0}{2}$ $T_b = T_2 + \frac{T_0}{2}$ $T_c = \frac{T_0}{2}$	$\bar{T}_a = \frac{T_0}{2}$ $\bar{T}_b = T_1 + \frac{T_0}{2}$ $\bar{T}_c = T_1 + T_2 + \frac{T_0}{2}$
2	$T_a = T_1 + \frac{T_0}{2}$ $T_b = T_1 + T_2 + \frac{T_0}{2}$ $T_c = \frac{T_0}{2}$	$\bar{T}_a = T_2 + \frac{T_0}{2}$ $\bar{T}_b = \frac{T_0}{2}$ $\bar{T}_c = T_1 + T_2 + \frac{T_0}{2}$
3	$T_a = \frac{T_0}{2}$ $T_b = T_1 + T_2 + \frac{T_0}{2}$ $T_c = T_2 + \frac{T_0}{2}$	$\bar{T}_a = T_1 + T_2 + \frac{T_0}{2}$ $\bar{T}_b = \frac{T_0}{2}$ $\bar{T}_c = T_1 + \frac{T_0}{2}$
4	$T_a = \frac{T_0}{2}$ $T_b = T_1 + \frac{T_0}{2}$ $T_c = T_1 + T_2 + \frac{T_0}{2}$	$\bar{T}_a = T_1 + T_2 + \frac{T_0}{2}$ $\bar{T}_b = T_2 + \frac{T_0}{2}$ $\bar{T}_c = \frac{T_0}{2}$
5	$T_a = T_2 + \frac{T_0}{2}$ $T_b = \frac{T_0}{2}$ $T_c = T_1 + T_2 + \frac{T_0}{2}$	$\bar{T}_a = T_1 + \frac{T_0}{2}$ $\bar{T}_b = T_1 + T_2 + \frac{T_0}{2}$ $\bar{T}_c = \frac{T_0}{2}$
6	$T_a = T_1 + T_2 + \frac{T_0}{2}$ $T_b = \frac{T_0}{2}$ $T_c = T_1 + \frac{T_0}{2}$	$\bar{T}_a = \frac{T_0}{2}$ $\bar{T}_b = T_1 + T_2 + \frac{T_0}{2}$ $\bar{T}_c = T_2 + \frac{T_0}{2}$

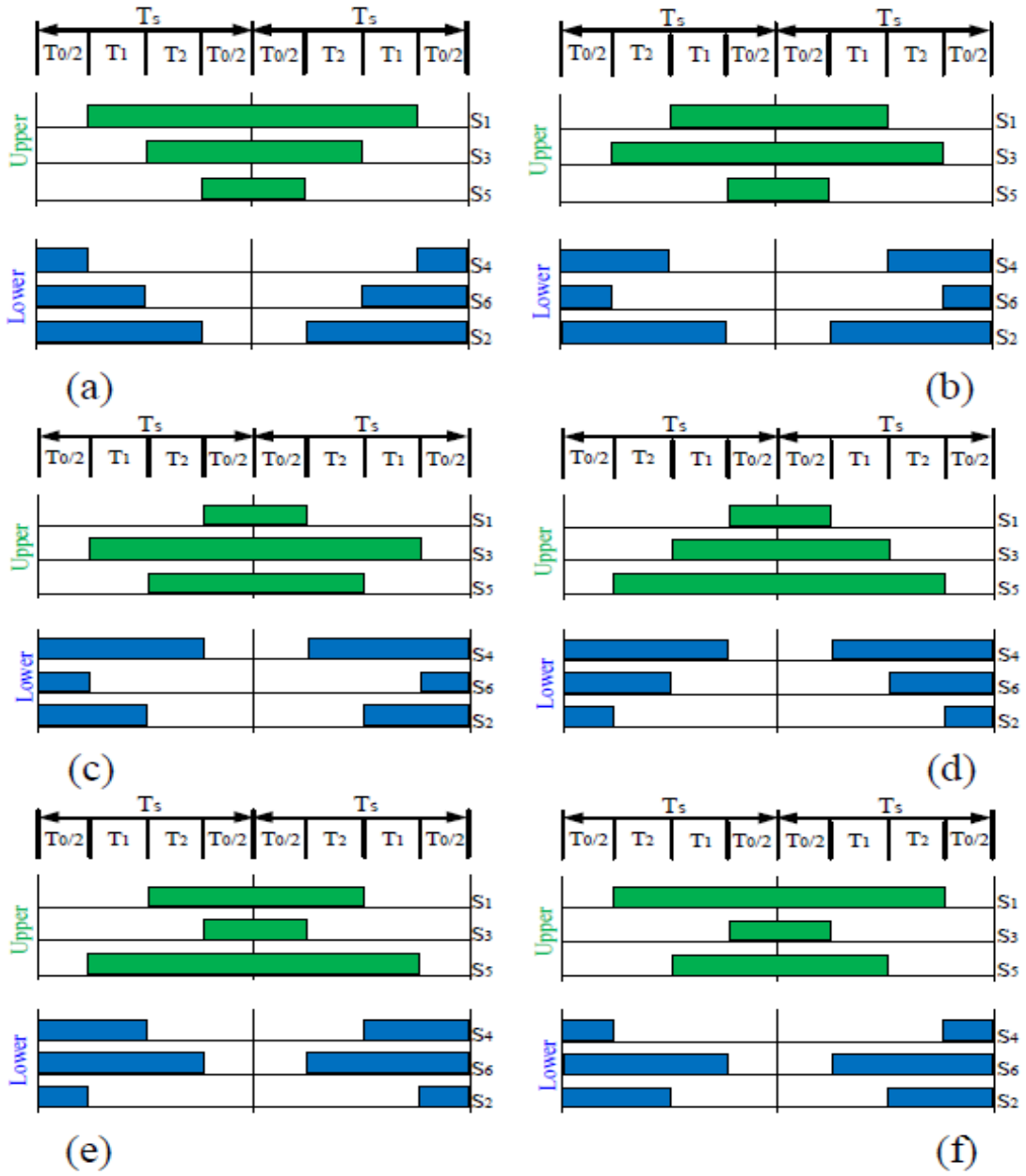

Figure 3.11. Switching by SVPWM method from sector 1 to sector 6 [44].

PART 4

METHODOLOGY

4.1. METAHEURISTIC OPTIMIZATION METHODS

In recent years, optimization algorithms are used as one of the modern and alternative methods of tuning controllers in electrical machines. Metaheuristic optimization methods are used for the purpose of finding a good solution to control the systems. Sometimes the solution may not be at an optimal level, but it is acceptable to some extent. Metaheuristic methods are iterative algorithms to address optimization problems. Thanks to these methods, the controllers can be designed due to the nonlinear structure of the system by simulation. They can be used in many engineering areas, such as power systems and industrial processes. Metaheuristic methods are algorithms based on exploration with a high search level to address optimization issues [22]. Optimization techniques are often used to improve the control performance of three phase IM. Usually, metaheuristic techniques are used to tune the PI speed controller gains due to their simplicity and free of mathematical complexity [45].

Metaheuristic methods are nature-inspired. For example, particle swarm optimization (PSO) method is developed by considering the behaviors of the birds. These methods provide practical, high-quality solutions at an acceptable time frame. They are iterative approaches that begin with a population of initial solutions, then produce a new population of solutions, and then integrate this new population into the present population using some selection proceedings. The iterative process finishes when reached in satisfactory state [46].

Metaheuristic algorithms are used commonly as essential tools for resolving optimization problems in a variety of engineering disciplines because of their

simplicity of them. Numerous algorithms have been presented in the literature such as Particle Swarm Optimization (PSO), Genetic Algorithm (GA), Artificial Bee Colony (ABC) algorithm, Differential Evolution (DE) algorithm, Grey Wolf Optimization (GWO), Ant Colony Optimizing (ACO), Cuckoo Search (CS) algorithm, etc. In order to determine the appropriate controller gains and improve the performance of an IFOC based IM drive, known PSO, GWO, and ABC algorithms are used in this thesis.

4.1.1. Particle Swarm Optimization (PSO)

Particle swarm optimization algorithm (PSO) is one method of the most popularly used optimization approaches. It has many advantages such as ease of implementation, ability of exploration, global convergence capability and strong robustness. In 1995 the PSO method developed by Eberhart and Kennedy was created by modeling the group behavior of birds [47]. In the PSO algorithm, the particles search the best solution in a defined and limited space. The PSO algorithm's fundamental idea is based on two primary considerations, namely the location and the velocity of the particles. The two equations below can be used to update these two factors [47]:

$$V^d{}_i(t+1) = wV^d{}_i(t) + c_1 r_1 \left(p^d{}_i(t) - x^d{}_i(t)\right) + c_2 r_2 (g^d{}_t(t) - x^d{}_i(t) \qquad (4.1)$$

$$x^d{}_i(t+1) = x^d{}_i(t) + V^d{}_i(t+1) \qquad (4.2)$$

Where *d* superscript shows the dimension of solution space which is determined by the number of optimized parameters. In this study, *d* is six due to the six optimized parameters which are three pairs of PI parameters applied to control the speed, *q*-axis component, and *d*-axis component of stator current. In above equations, *i* subscript shows the current particle and *t* is the current iteration, x is the location of the particle, p is the local best position which means the best position of each particle, g is the global best position which means the best position for each optimized parameters, $r_1 and\ r_2$ are the random values between 0 and 1, while *w* is the inertia

factor, $c_1 \, and \, c_2$ which pull the particle to local and global best positions, are constants and *V* is the velocity of the particle.

The stages of the PSO algorithm can be summed up as follows:

- A random population is determined in the defined and limited search space.
- The fitness values of the particles are evaluated by using the objective function.
- The local best position and global best position are determined.
- The new velocities of the particles are determined by using Equation (4.1).
- The new positions of the particles are determined by using Equation (4.2).
- The optimization procedure is repeated by starting from step 2 until the end of the iterations.

At the end of the iterations, the global best position can be considered as the optimal solution for the issue [48]. Figure 4.1 shows the flowchart of PSO algorithm [49].

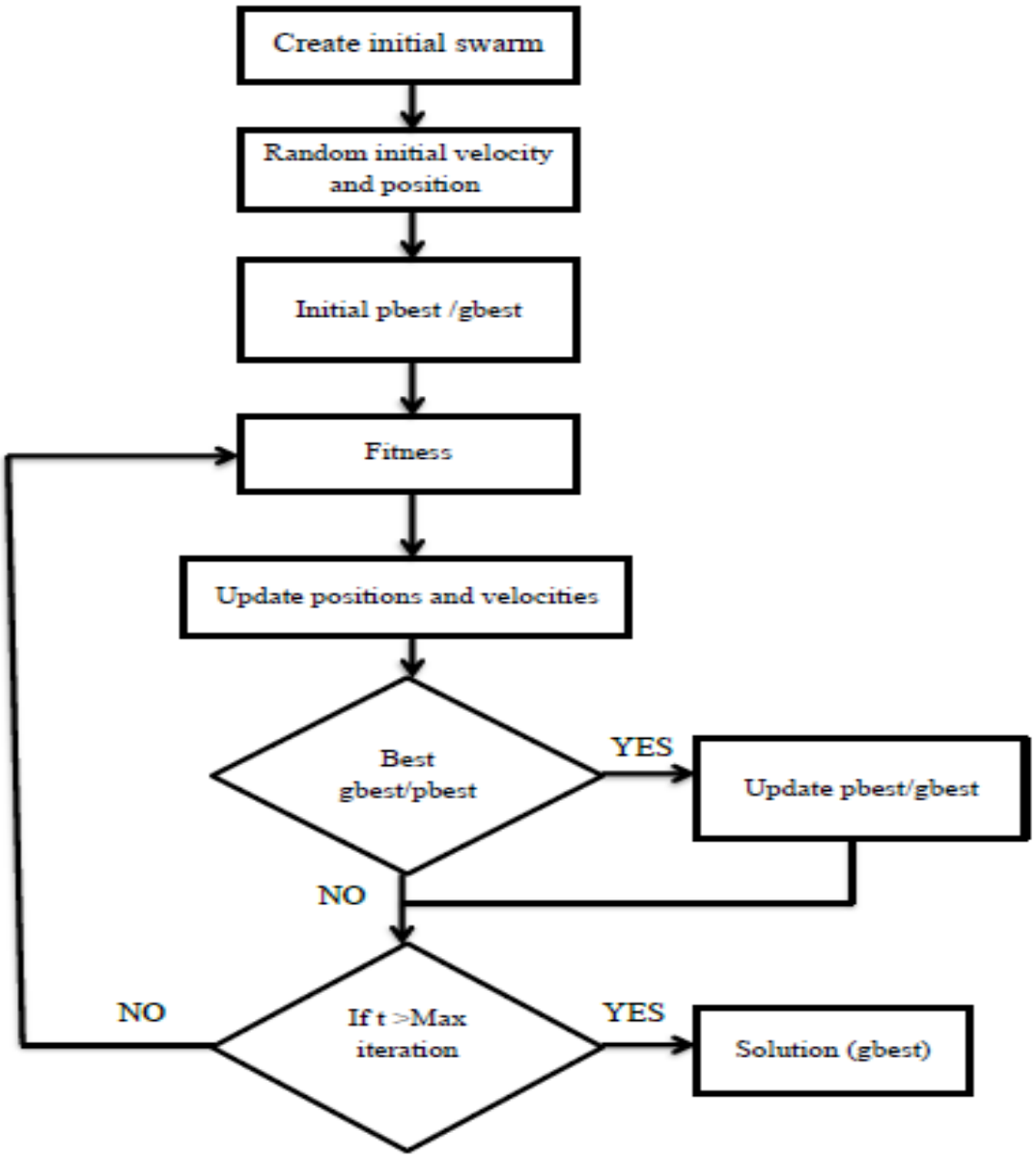

Figure 4.1. PSO flowchart.

c_1 and c_2 acceleration constants and the inertia factor are crucial for the PSO algorithm performance. With the help of these parameters, the swarm particles jump to the appropriate location and reduce the time to half. As PSO algorithms have developed, the inertia weight idea has been incorporated as a constant parameter that gives momentum to the swarm of particles. When inertia values are large, a greater global search feature is provided. When inertia values are low, an effective local search feature is provided [49].

4.1.2. Grey Wolf Optimization (GWO)

Mirjalili et al. introduced Grey Wolf Optimization (GWO) algorithm in 2014 [50]. In recent years, GWO algorithm has been widely used in the optimization problems. This algorithm simulates the hunting function of the grey wolves existing in the nature. GWO algorithm starts to search with a population of wolves generated randomly. The leadership structure is shown below in Fig. 4.2 by four various types of grey wolves designated as alpha, beta, delta, and omega. The alphas are in charge of making judgments regarding hunting, sleeping locations, wake-up times, and other issues. Decisions made by the alphas are communicated to the group through betas. Although the alphas are not the strongest members of the group, they are the greatest whence managerial abilities. The betas assist the alphas in decision-making and participating in other group activities. Omega is the grey wolf with the lowest ranking. All other dominant wolves always control the omega wolves which are considered the last wolves that are allowed to consume food. While the delta wolves are subject to alpha and beta wolves, other types rule the omega [50].

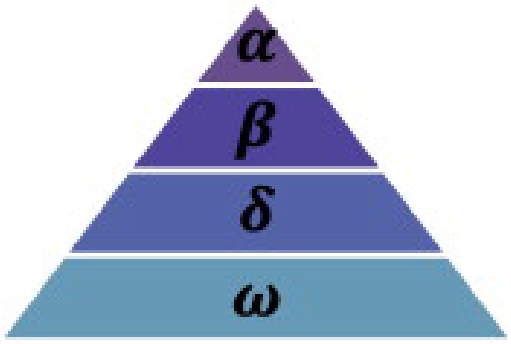

Figure 4.2. Grey wolf social structure [50].

Grey wolves hunt in three primary stages: looking for prey, surrounding prey, and attacking prey. In order to create GWO to execute optimization, Grey wolf social structure and hunting strategy are mathematically modeled. By using this technique, the population is split into four different groups: alpha (α), beta (β), delta (δ), and omega (ω) in order to establish the social structure of wolves during a GWO design. The first three ideal solutions after iterations are designated as α, β, and δ, respectively. The hunt (optimization) in the GWO algorithm is directed by α, β, and

δ. To obtain best solutions, the ω wolves must be following these different three wolf types. These steps can be used to simulate the encircling process [50].

$$\bar{D} = \left|\bar{C}.\overline{X_p}(t) - \bar{X}(t)\right| \tag{4.3}$$

$$\bar{X}(t+1) = \bar{X}(t) - \bar{A}.\bar{D} \tag{4.4}$$

Where t is the current iteration, $\overline{X_p}$ is the location vector of the prey, $\bar{X}$ is the location vector of the grey wolf, $\bar{A}$=2$\bar{a}.\bar{r_1} - \bar{a}$, $\bar{C} = 2\bar{r_2}$, $\bar{a}$ is linearly reduced during the iterations from number 2 to 0, and r_1 and r_2 denote random numbers between [0, 1]. We always assume that α, β, and δ has more information about the location of the prey to mimic the hunting strategy of grey wolves mathematically. Therefore, the first three best solutions (α, β, δ) obtained are saved in their current positions and the locations of the other wolves are updated according to the location of α, β, and δ. The following formulas are given in this regard.

$$\overline{D_\alpha} = |\overline{C_1}.\overline{X_\alpha} - \bar{X}| \tag{4.5}$$

$$\overline{D_\beta} = \left|\overline{C_2}.\overline{X_\beta} - \bar{X}\right| \tag{4.6}$$

$$\overline{D_\delta} = |\overline{C_3}.\overline{X_\delta} - \bar{X}| \tag{4.7}$$

$$\overline{X_1} = \overline{X_\alpha} - \overline{A_1}.(\overline{D_\alpha}) \tag{4.8}$$

$$\overline{X_2} = \overline{X_\beta} - \overline{A_2}.\left(\overline{D_\beta}\right) \tag{4.9}$$

$$\overline{X_3} = \overline{X_\delta} - \overline{A_3}.(\overline{D_\delta}) \tag{4.10}$$

$$\bar{X}(t+1) = \frac{\overline{X_1} + \overline{X_2} + \overline{X_3}}{3} \tag{4.11}$$

The convergence and divergence of the wolves in the exploration process depend on the value of the $\vec{A}$. If $|\vec{A}| > 1$, it means that the wolves should keep away from each other to find the best prey. If $|\vec{A}| < 1$, it means that the wolves must attack the prey. The flowchart of GWO algorithm is shown below [45].

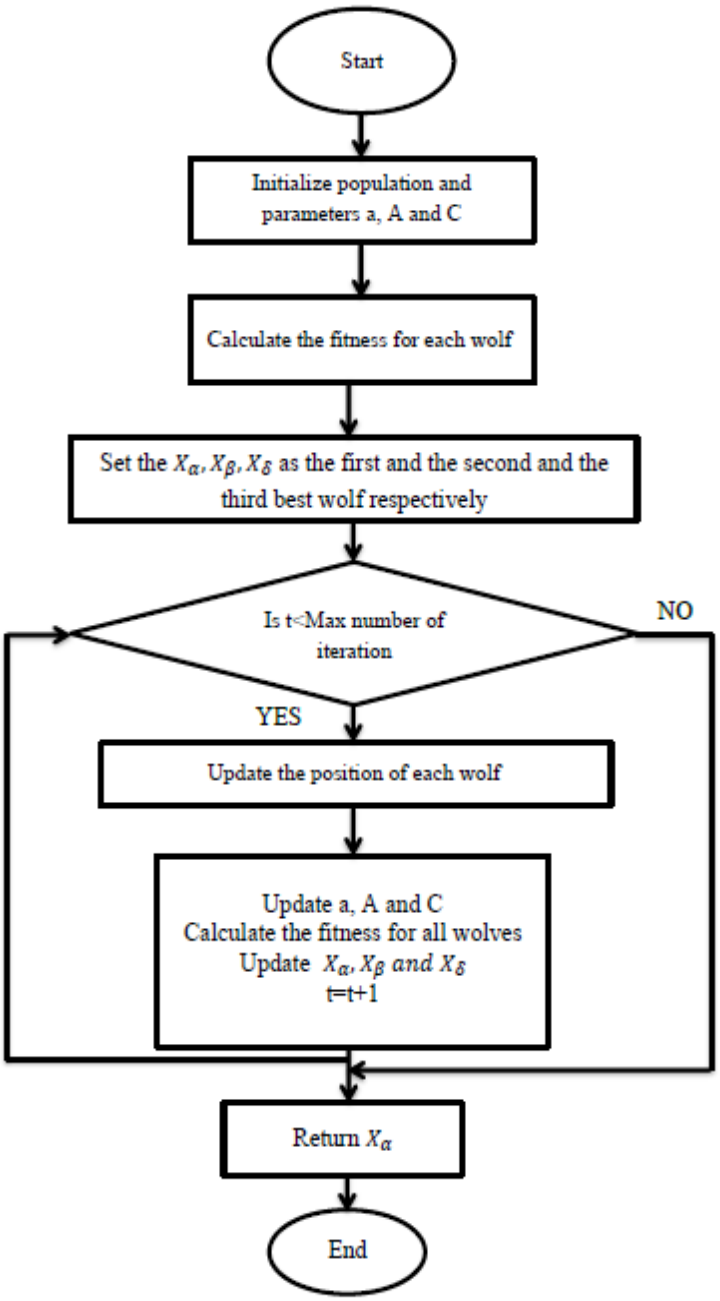

Figure 4.3. GWO flowchart.

4.1.3. Artificial Bee Colony (ABC)

Artificial Bee Colony (ABC) algorithm is an effective method for optimization issues. This technique is being employed in numerous applications of real-world. Karaboga proposed the ABC algorithm in 2005 [51]. This algorithm is based on the behavior of honeybee and offers us a powerful tool to solve complex optimization issues. In this algorithm, there are three categories of artificial bees in the colony: scout bees, employed bees, and onlooker bees. Scout bees scan the environment randomly for undiscovered food sources. Employed bees find food sources, transport it to the hive, and share its location with other bees. Onlooker bees go to the sources according to the information provided by the employed bees and evaluate the quality of food. In the ABC algorithm, the location of each food source defines a point in the problem domain (i.e., a potential solution). The initial population of SN solutions (food sources) is generated at random. The n^{th} solution is represented by the following equation [51].

$$X_n = \left[X_{n,1}, X_{n,2}, \ldots . X_{n,m}\right] \tag{4.12}$$

Where SN is the number of food sources, and m denotes the number of parameters to be optimized. By using the following equation, the employed bees identify neighbor food sources in the nearness the food source.

$$V_{n,i} = X_{n,i} + \varphi_{n,i}\left(X_{n,i} - X_{k,i}\right) \tag{4.13}$$

Where k ($k \neq n$) is an integer selected at random in the range [1, SN], $\varphi_{n,i}$ is a random number chosen from the range [1, 1], i is a dimension index chosen randomly from the range of [1, m]. If V_n has a fitness value better than X_n, X_n is updated with V_n. Otherwise, X_n does not change.

After the finished of the search process by the employed bees, they share with the onlooker bees the location of the food sources. Then, a selection process is performed by the onlooker bees using the quality of food which is determined by the

nectar amount. This process is performed by the roulette wheel method given by Equation 4.14.

$$P_n = \frac{fit_n}{\sum_{k=1}^{SN} fit_k} \tag{4.14}$$

Where fit_n denotes the n^{th} solution of the fitness value. The fitness value means the quality of food source. In this method, if there is no improvement through a specified number of subsequent trials of food source, the employed bee abandons that food source, and the employed bee for this food source changes to a scout bee. The scout bee discovers a new food source which is produced randomly in the predefined limit as shown in Equation 4.15 [52].

$$X_{n,i} = X_i^{min} + rand[0,1]\left(X_i^{max} - X_i^{min}\right) \tag{4.15}$$

The schematic flowchart of ABC algorithm is presented below:

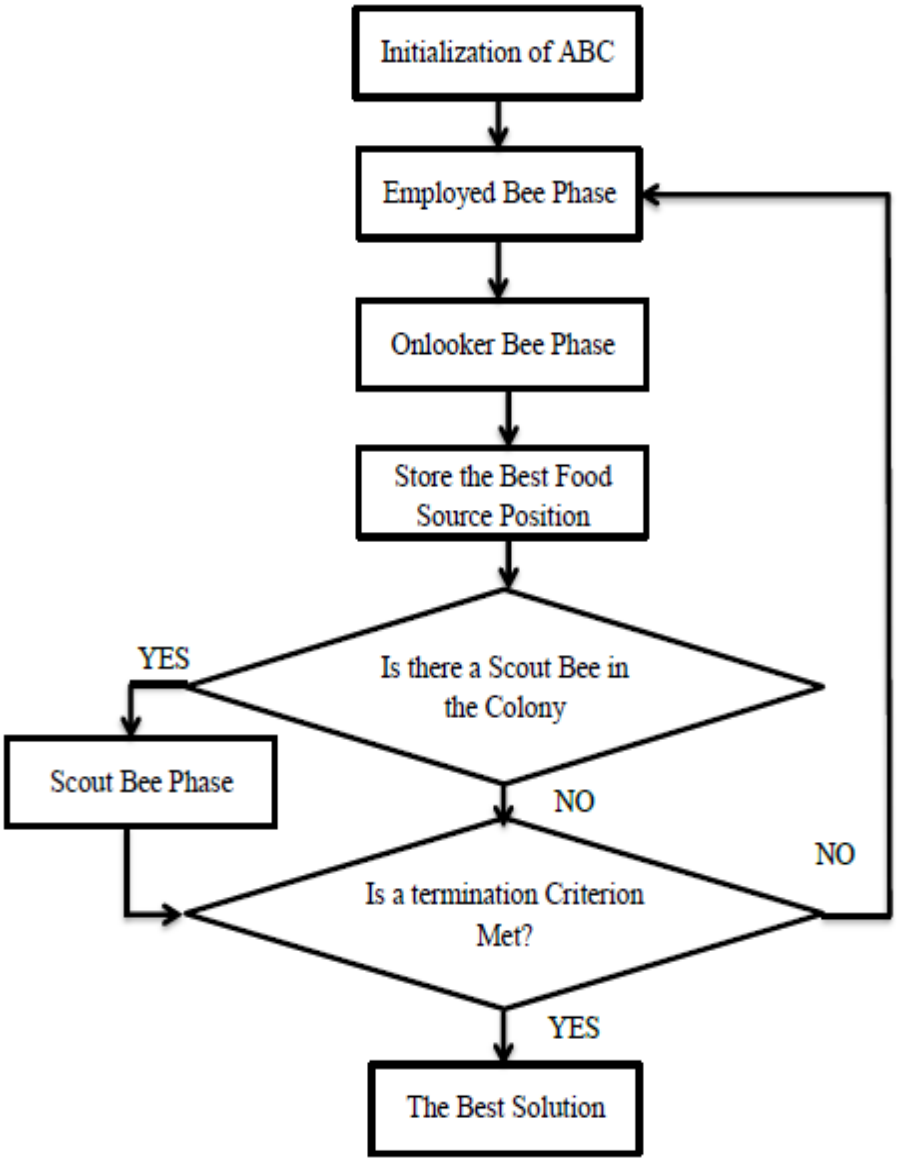

Figure 4.4. ABC Flowchart.

PART 5

SIMULATION RESULTS AND DISCUSSION

In the FOC system, speed, torque, and flux are controlled. However, flux and torque are controlled by the components of stator current. As a result, FOC system contains three control loops for controlling speed, quadrature (q) and direct (d) components of stator current. Generally, as mentioned in the previous chapters, PI controllers are used in these control loops belong to FOC system. In this thesis, some metaheuristic algorithms such as PSO, GWO and ABC are applied to optimize K_p and K_i controller gains for the purpose of improving the performance of FOC based IM. The simulation results obtained by MATLAB are presented for three different operating conditions which are no-load condition, speed change condition and sudden load change condition. The obtained results will be discussed in this section.

The used induction motor parameters are given in Table 5.1.

Table 5.1. Induction motor parameters.

Parameter	Value
Power	5.5 KW
Number of pole (P)	4
Stator resistance ($\mathbf{R_s}$)	1.28333Ω
Rotor resistance ($\mathbf{R_r}$)	0.9233Ω
Stator inductance ($\mathbf{L_s}$)	0.141833H
Rotor inductance ($\mathbf{L_r}$)	0.143033H
Mutual inductance (M)	0.137333H
Inertia torque (J)	0.1 kg/m^2
Friction coefficient (f_d)	0.0028 Nm s/rad

In the metaheuristic algorithms, the fitness value is calculated according to the objective function. As a result, to determine objective function has a crucial role to solve optimization problems. As the performance of FOC based IM is determined

due to the mentioned three control loops, objective function given by Equation (5.1) which is adopted for the optimization process, consists of three terms based on Sum of Absolute Errors (SAE) index, being related to minimizing speed (e_ω), d component of stator current (i_{sd}) and q component of stator current (i_{sq}) errors. $w_{1,2,3}$ are weighting factors used to equalize the three terms in the same magnitude order.

In this study, we obtained the values of the weighting factor (w_1=1, w_2=24 and $w_3 = 24$) by trial and error. However, the weighting factors can also be determined according to the Pareto method which is utilized in the literature by [53] [54].

$$f_{cost} = w_1 SAE_\omega + w_2 SAE_{isd} + w_3 SAE_{isq} \tag{5.1}$$

SAE function for any variable is shown below by the following equation.

$$SAE_x = \sum_{i=1}^{N} |x_r(i) - x_m(i)| \tag{5.2}$$

Where x_r and x_m show the reference and measured values respectively for x variable, and *N* is the element number of x variable.

The parameters of used PSO algorithm are shown in Table 5.2.

Table 5.2. PSO algorithm parameters.

Parameter	Value
Dimension size	6
Population size	50
Maximum inertia weight	0.9
Minimum inertia weight	0.4
Acceleration factors (c_1, c_2)	2.05
Iteration size	100

The optimized PI controller gains obtained by PSO algorithm are given for speed, i_{sq} and i_{sd} control in Table 5.3.

Table 5.3. PSO- PI controller gains

Controller	K_p	K_i
Speed controller	5.7647	500
$\boldsymbol{i_{sq}}$ **controller**	3.9903	1700
$\boldsymbol{i_{sd}}$ **controller**	6.9523	1170.1339

The parameters of used ABC algorithm are shown in Table 5.4.

Table 5.4. ABC algorithm parameters.

Parameter	Value
Dimension size	6
Population size	50
Iteration size	100

The optimized PI controller gains obtained by ABC algorithm are given for speed, i_{sq} and i_{sd} control in Table 5.5.

Table 5.5. ABC PI controller gains.

Controller	K_p	K_i
Speed controller	6.36	500
$\boldsymbol{i_{sq}}$ **controller**	4.1922	1672.5
$\boldsymbol{i_{sd}}$ **controller**	6.9062	1144.8

However, the parameters of used GWO algorithm are shown in Table 5.6.

Table 5.6. GWO algorithm parameters.

Parameter	Value
Dimension size	6
Population size	50
Iteration size	100

The optimized PI controller gains obtained by GWO algorithm are given for speed, i_{sq} and i_{sd} control in Table 5.7.

Table 5.7. GWO PI controller gains.

Controller	K_p	K_i
Speed controller	6.6021	500
i_{sq} controller	4.2106	1663.9
i_{sd} controller	6.8391	1163.2

5.1. NO LOAD CONDITION

Firstly, the FOC based IM was operated at no load condition when the reference speed was 75 rad/s. The speed responses by the metaheuristic algorithms are given in Figure 5.1.

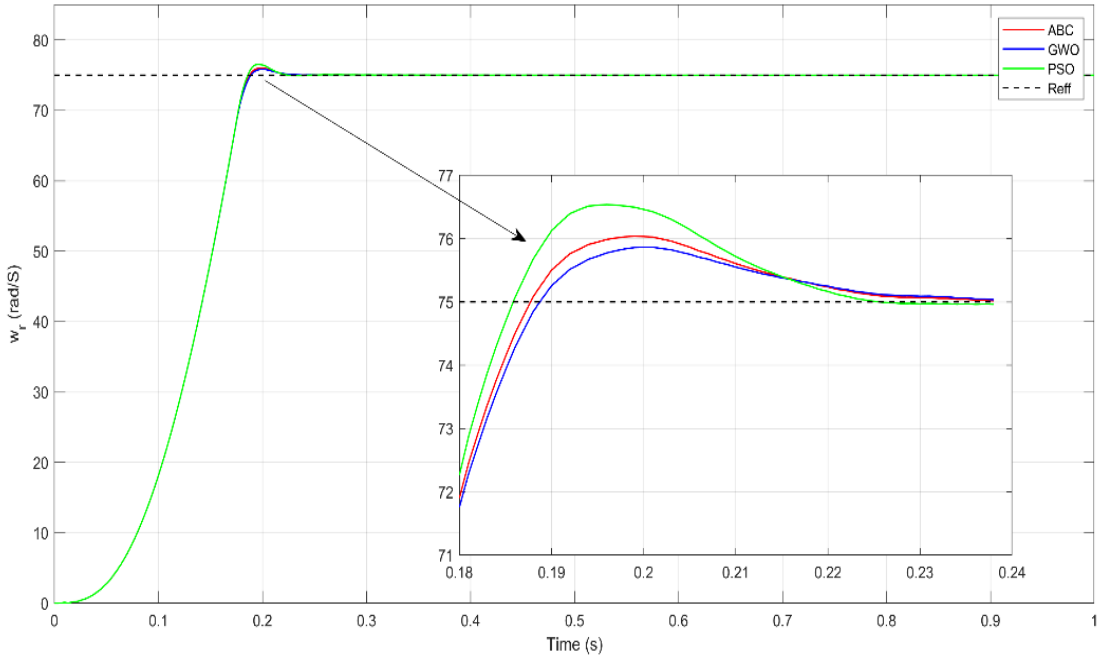

Figure 5.1. Speed at no load condition.

Table 5.8 shows the performances of the used metaheuristic methods. The motor speed reaches at the desired speed after about 0.183 seconds by GWO and ABC methods, when that time of PSO method is about 0.198 seconds. The settling time of GWO and ABC is 0.15 seconds shorter than that of PSO. While the maximum overshoot (2.05 %) is seen by PSO method, the minimum overshoot (1.15 %) is seen

by GWO method. So, the overshoot with GWO is lower than other methods. However, the rising time of the methods is the same. The speed controller performance by GWO optimization algorithm is the best. Also, it may be said that the ABC method performs better than the PSO method.

Table 5.8. Comparison between the responses of different algorithms at no load speed.

	Rise Time (s)	**Settling time (s)**	**Peak overshoot (%)**
PSO	0.1024	0.1988	2.05
GWO	0.1024	0.1838	1.15
ABC	0.1024	0.1833	1.39

For the same simulation conditions, while the i_{sd} current controller performance is shown in Figure 5.2, the i_{sq} current controller performance is shown in Figure 5.3 based on each optimization method**.** The most important intervals are zoomed in to show the difference in the controller performance for each optimization algorithm.
For both current controllers, it is seen that the results of the three optimization methods do not differ significantly**.**

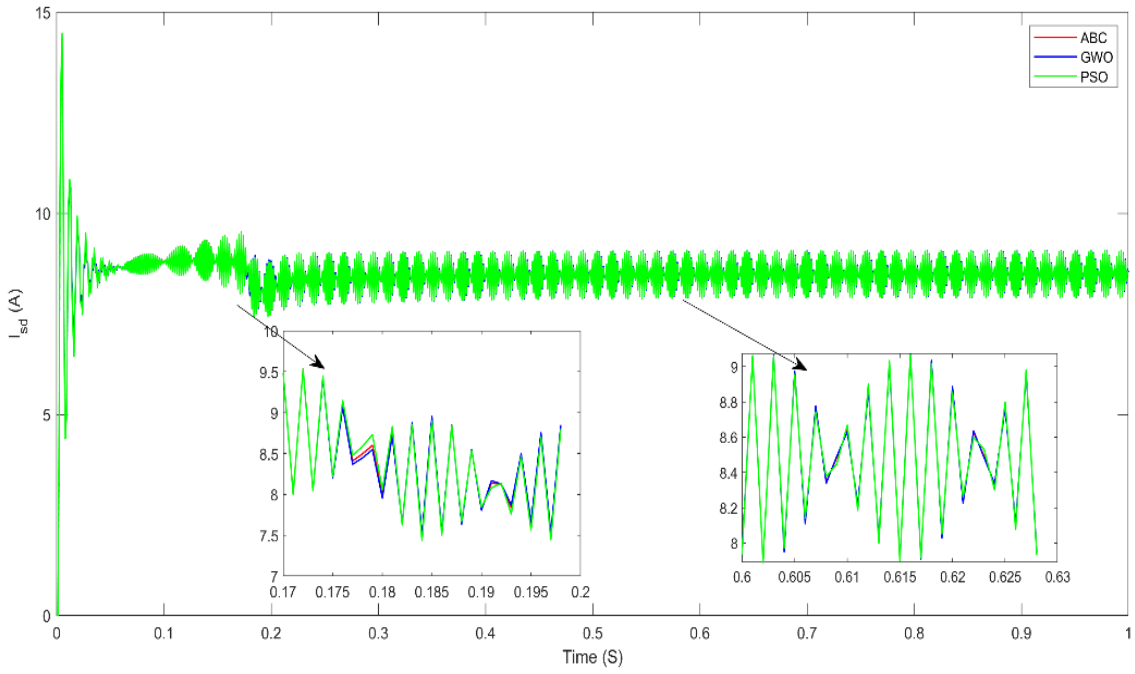

Figure 5.2. i_{sd} at no load condition.

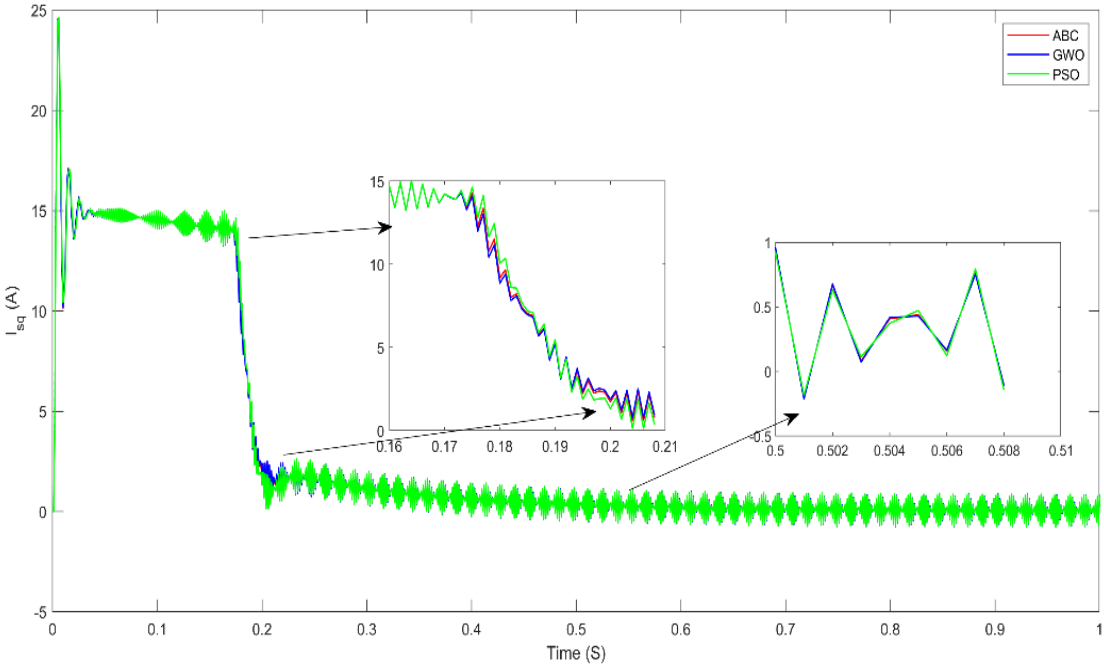

Figure 5.3. i_{sq} at no load condition.

5.2. SPEED CHANGE CONDITION

Secondly, the performances of the methods are examined under the variable speed condition. At the beginning, the reference speed is 75 rad/sec. It is increased to 150 rad/sec at the time of 1th second. Lastly, the reference speed is decreased from 150 rad/sec to -150 rad/sec at the time of 4th second to examine the performance when the rotation direction of IM is changed. The speed response is given by Figure 5.4. As you can see, the control capability of the methods is good under the variable reference speed condition. Also, PI speed controller by metaheuristic methods can control the FOC based IM when the rotation direction of IM is changed. There are three transient cases in this test. In all transient cases, GWO optimization algorithm is the best among the three methods. The peak overshoot is 0.67 % in the second transient case by GWO, while it is 0.55 % in the third transient case by the same algorithm. Selected time intervals are zoomed in to show the controller performances.

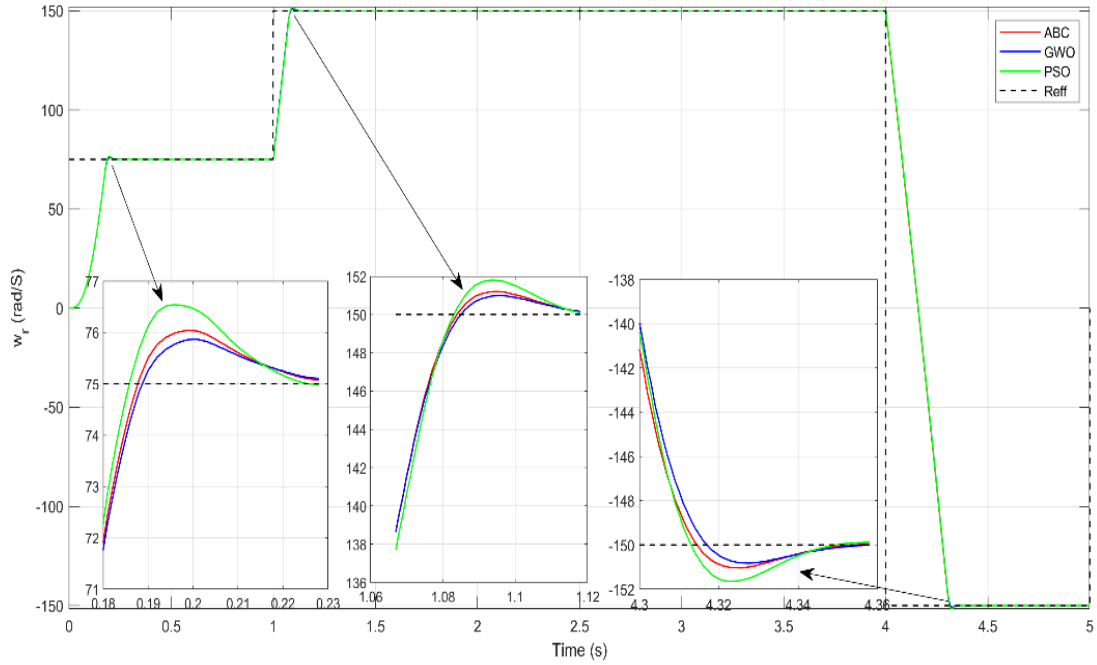

Figure 5.4. Speed at change condition.

On the other hand, i_{sd} current graphic is shown in Figure 5.5. In steady state condition, i_{sd} current varies between 7 A and 10 A by all metaheuristic methods. When the speed of the IM is increased to 150 rad/sec from 75 rad/sec, i_{sd} current ripple increases.

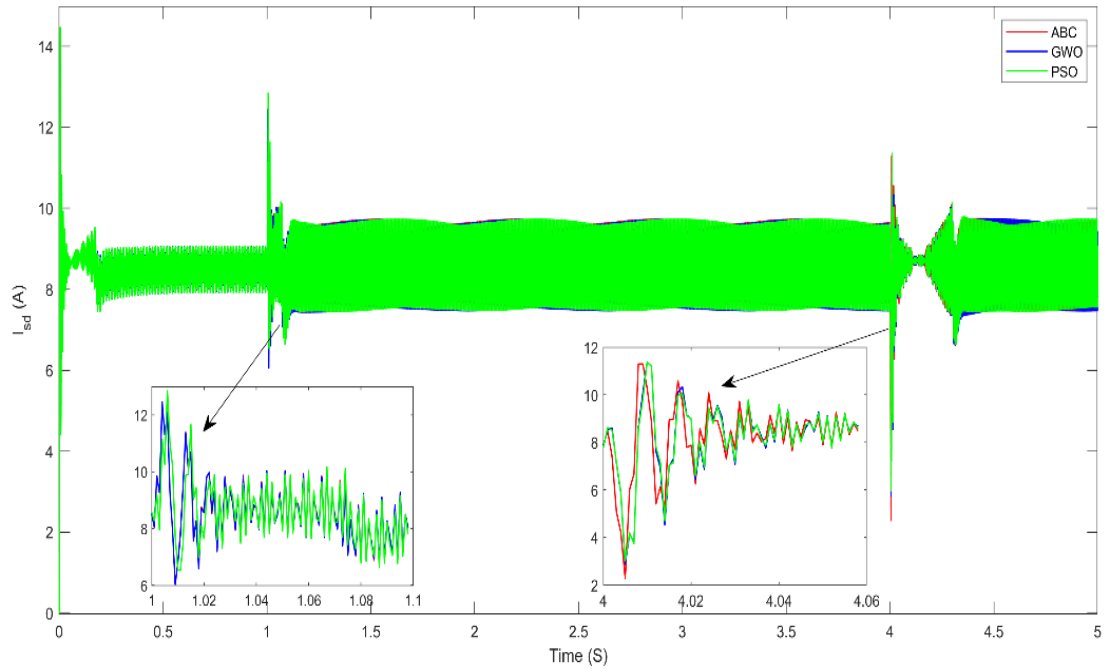

Figure 5.5. i_{sd} at change condition.

Figure 5.6 shows the i_{sq} current response under the variable speed condition for the three optimization methods. As shown in mentioned figure, there is no considerable difference among the three curves even in transient conditions. The steady state value of i_{sq} current for all optimization methods is near to zero. In addition, i_{sq} current ripple increases when the speed of IM increases.

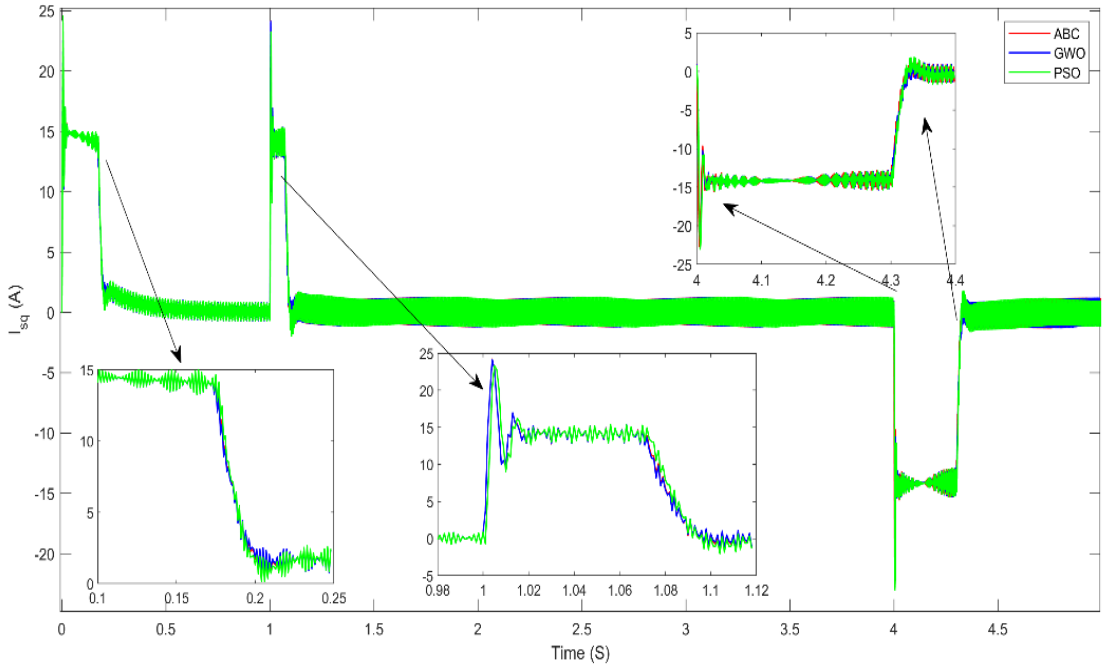

Figure 5.6. i_{sq} at change condition.

5.3. SUDDEN LOAD CHANGE CONDITION

The sudden load change test is also realized by the used optimization methods for FOC based IM. While the reference speed is 150 rad/sec, the load torque is increased to 25 Nm from 0 Nm at the 1st second and it is decreased to 10 Nm from 25 Nm at the 2nd second.

Figure 5.7 shows the speed responses provided by PI speed controller of which gains are tuned via optimization by metaheuristic algorithms. At the 1st second, the speed of IM decreases because of increased load torque, and it reaches at the reference speed after a short transient time. At the 2nd second, the speed of IM increases due to the reduced load, and it reaches a steady state at the desired speed. As a result, speed

control is achieved successfully by all methods. However, at the sudden load change points, it is seen that speed response is less affected by GWO and ABC algorithm. Due to the load disturbance, in the second transient case, the speed of IM reaches at the desired speed (150 rad/s) after 0.084 seconds and 0.088 seconds by ABC and GWO, respectively, while that time is 0.074 seconds by PSO. In the third transient case, that times are 0.081 seconds, 0.085 seconds, and 0.074 seconds by ABC, GWO and PSO respectively. So, it can be said that the settling time in the transient case due to load disturbance is minimum by PSO.

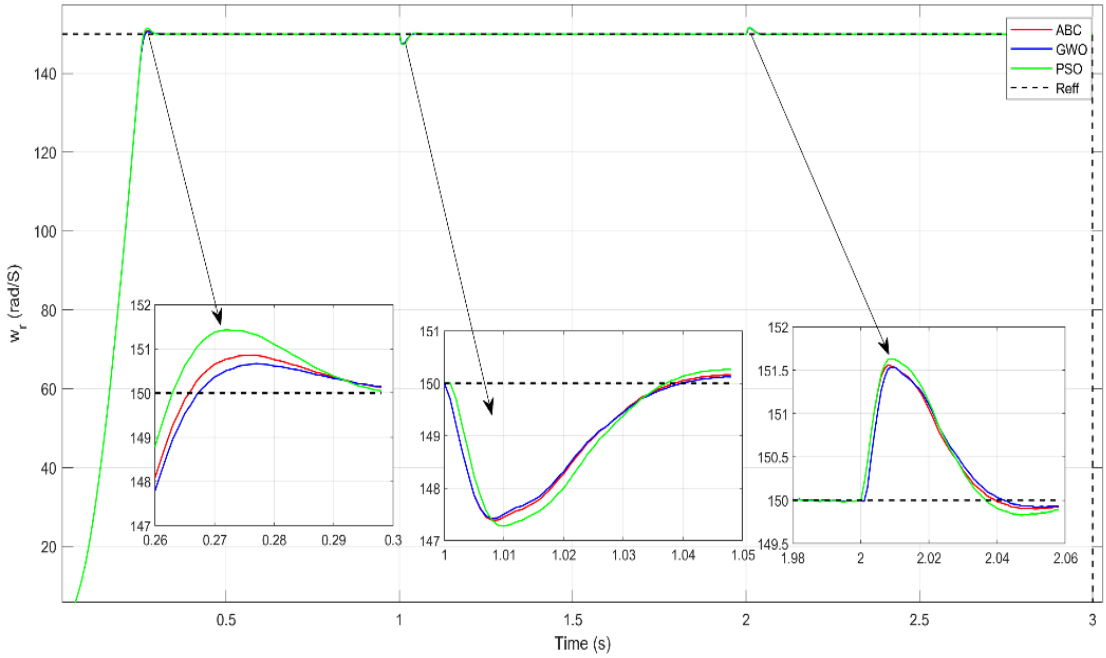

Figure 5.7. Speed at sudden load condition.

Figures 5.8 and 5.9 respectively show the i_{sd} and i_{sq}current responses under the same operation condition. The responses are almost the same by all metaheuristic methods. According to the steady state values, it can be noted that i_{sd} current value does not change very much, but i_{sq} current is affected significantly. Because increased load torque causes increased electromagnetic torque. As the electromagnetic torque is controlled by i_{sq} current in FOC of IM, increased load torque causes increased i_{sq} current as seen in Figure 5.9. So, it is normal that reduced load torque causes a lower i_{sq} current. When the load torque is increased to 25 Nm

from 0 Nm, i_{sq} current value increases to 8 A from 0 A. When it is reduced to 10 Nm from 25 Nm, i_{sq} current value decreases to 3 A from 8 A.

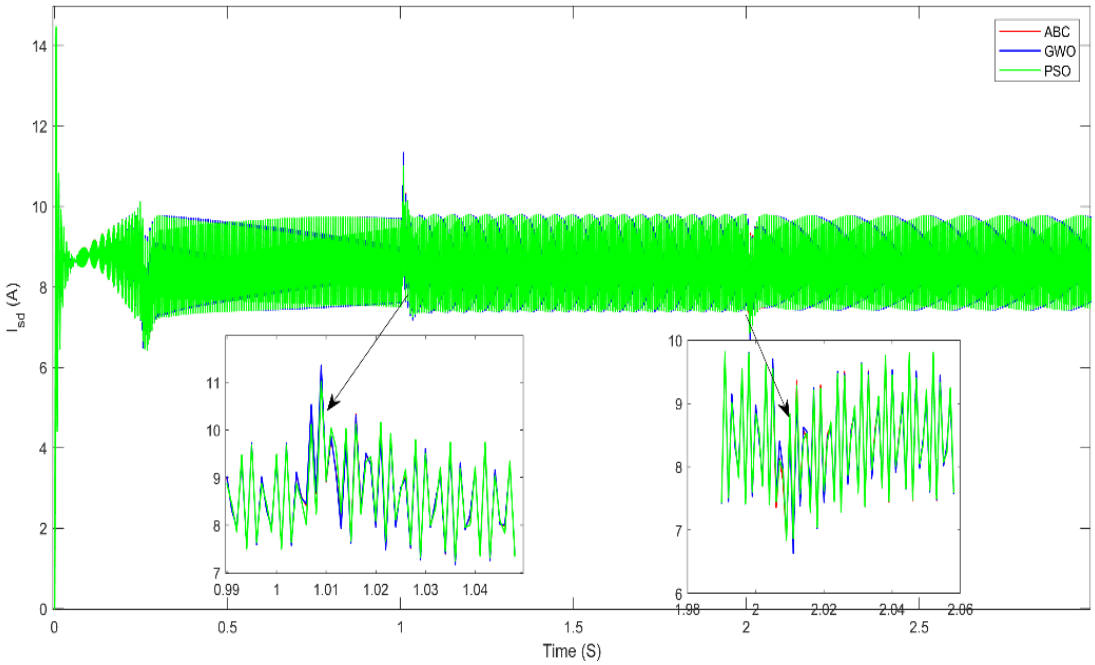

Figure 5.8. i_{sd} at sudden load condition.

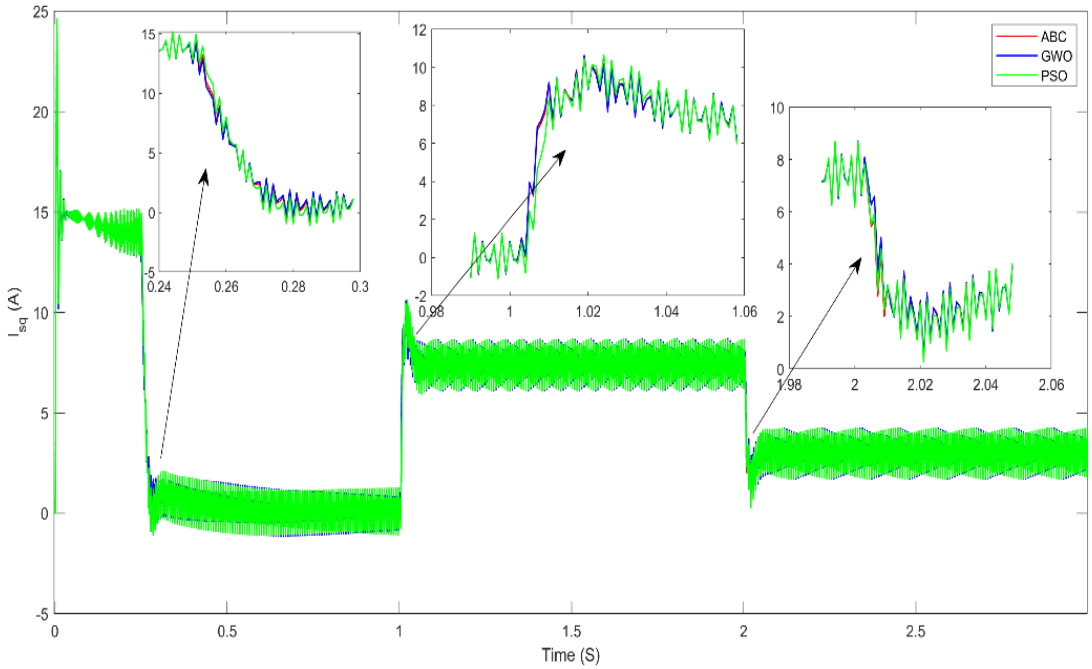

Figure 5.9. i_{sq} at sudden load condition.

Figure 5.10 shows the convergence speed of PSO, ABC and GWO algorithm. It is seen that while ABC algorithm converges to the optimal result at the 34th iteration, GWO algorithm converges at the 72nd iteration and PSO converges at the 41st iteration. Therefore, it can be noted that ABC algorithm is the best and GWO is the worst between the three algorithms in terms of convergence speed.

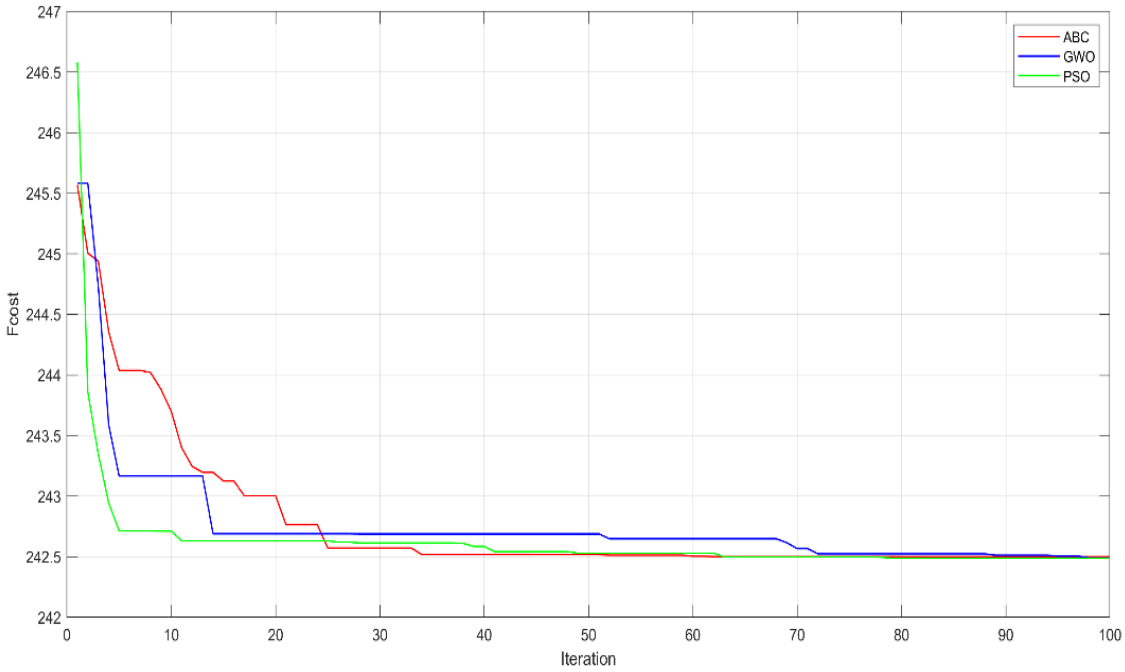

Figure 5.10. Convergence speed of metaheuristic algorithms.

PART 6

CONCLUSION AND FUTURE WORK

6.1. CONCLUSION

In this thesis, simulation of IFOC based IM is realized by MATLAB. As the IFOC method includes 3 PI controllers for speed control and *d-q* currents control, the gains of all PI controllers are optimized by the metaheuristic algorithms (PSO, GWO and ABC) to improve the dynamic performance of IM. The evaluation is made due to the responses of IM under three operating conditions which are no load condition, speed change condition and sudden load change condition. At the no load and speed change conditions, the best dynamic performance especially in terms of maximum overshoot is obtained by GWO algorithm. At the speed change test, although the rotation direction of IM is changed, the control capability of the used controllers is good. However, the *d-q* current responses are almost the same by used all metaheuristic algorithms. At the load change condition, the speed response is less affected by GWO and ABC algorithm due to the load disturbance. However, settling time in the transient cases due to load disturbance is minimum by PSO. When load torque is increased, it causes the increased i_q current value.

Therefore, the optimization of the gains of PI controllers in IFOC based IM is achieved successfully by the utilized metaheuristic techniques. The metaheuristic method creates highly efficient optimization processes and the capacity to find the optimal solution quickly and precisely, replacing with "trial and error" methods, which are time-consuming, difficult, and produce subpar results. The outcomes demonstrated that the dynamic performance with GWO algorithm is better and more robust than that with PSO and ABC in IFOC based IM. However, the convergence speed of GWO algorithm to the optimal results is slower than PSO and ABC algorithms.

6.2. FUTURE WORK

In the future work, recent important metaheuristic algorithms such as red fox optimization algorithm can be applied and compared with GWO algorithm for IFOC based IM. Also, the dynamic performance of IM can be improved by combining the metaheuristic methods. Because a hybrid optimization method will eliminate the disadvantage of each one of the methods. In addition, in IFOC based IM, an adaptive fuzzy logic controller of which membership functions are tuned by metaheuristic methods, can be used instead of PI controllers to improve the dynamic performance.

REFERENCES

[1] Ferdiansyah, I., Rusli, M. R., Praharsena, B., Toar, H., and Purwanto, E., "Speed control of three phase induction motor using indirect field oriented control based on real-time control system" ***, In 2018 10th International Conference on Information Technology and Electrical Engineering (ICITEE),*** pp. 438–442, (2018).

[2] Theraja, B. L., *et al.*, "A textbook of electrical technology vol ii", ***S. Chand Publ.,*** (2005).

[3] Chapman,S. J., "Electric machinery fundamentals fifth edition" ,***Mcgraw-hill***, inc., (2012).

[4] Filizadeh, S., " Electric machines and drives: principles, control, modeling, and simulation" ***,CRC Press***, (2013).

[5] Martinez-Hernandez, M. A., Gutierrez-Villalobos, J. M., Malagon-Soldara, S. M. Mendoza-Mondragon, F. and Rodriguez-Resendiz, J. "A speed performance comparative of field oriented control and scalar control for induction motors," ***in 2016 IEEE Conference on Mechatronics, Adaptive and Intelligent Systems (MAIS)***, pp. 1–7, (2016).

[6] Febin, D. JL., Subbiah, V., Iqbal, A., and Padmanaban, S. "Novel wavelet-fuzzy based indirect field oriented control of induction motor drives," ***J. Power Electron.,*** vol. 13, no. 4, pp. 656–668, (2013).

[7] Aziri, H., Patakor, F. A., Sulaiman, M., and Salleh, Z. "Comparison Performances of Indirect Field Oriented Control for Three-Phase Induction Motor Drives," ***Int. J. Power Electron. Drive Syst.,*** vol. 8, no. 4, p. 1682, (2017).

[8] Zhang,Y., Jiang, Z., and Yu, X., "Indirect field-oriented control of induction machines based on synergetic control theory," **in *2008 IEEE Power and Energy Society General Meeting-Conversion and Delivery of Electrical Energy in the 21st Century,*** pp. 1–7, (2008).

[9] Kumar A., and Ramesh, T., "Direct field oriented control of induction motor drive," ***in 2015 Second International Conference on Advances in Computing and Communication Engineering,*** pp. 219–223, (2015).

[10] Yousef, A. Y., and Abdelmaksoud, S. M. "Review on field oriented control of induction motor," ***Int. J. Res. Emerg. Sci. Technol.(IJREST),*** vol. 2, pp. 5–16, (2015).

[11] Goyat, S., and Ahuja, R. K. “Speed control of induction motor using vector or field oriented control,” ***Int. J. Adv. Eng. Technol.***, vol. 4, no. 1, p. 475, (2012).

[12] Nishad, B. K., and Sharma, R., “Induction motor control using modified indirect field oriented control,” **in *2018 8th IEEE India International Conference on Power Electronics (IICPE)***, pp. 1–5, (2018).

[13] Trzynadlowski, A. M., “Control of induction motors” ***Elsevier,*** (2000).

[14] Ha,V. T., Lam, N. T. Ha, V. T., and Vo, Q. V., “Advanced control structures for induction motors with ideal current loop response using field oriented control,” ***Int. J. Power Electron. Drive Syst.,*** vol. 10, no. 4, p. 1758, (2019).

[15] Banerjee, T., Choudhuri,S., Bera, J., and Maity, A. “Off-line optimization of PI and PID controller for a vector controlled induction motor drive using PSO,” **in *International Conference on Electrical & Computer Engineering (ICECE 2010)***, pp. 74–77**,** (2010).

[16] Lai, C., Peng, K., and Cao, G., “Vector control of induction motor based on online identification and ant colony optimization,” **in *2010 2nd International Conference on Industrial and Information Systems***, vol. 2, pp. 206–209**,** (2010).

[17] Sharifian, M. B. B., Galvani, S., and Kouhshahi, M. B., “Torque fluctuations reducing in a vector-controlled induction motor drive by PI controller tuning using particle swarm optimization,” **in *2011 International Conference on Electrical Machines and Systems***, pp. 1–6, (2011).

[18] Bohari, A. A., Utomo, W. M., Haron, Z. A., Zin, N. M., Sim, S. Y., and Ariff, R. M. “Speed tracking of indirect field oriented control induction motor using neural network,” ***Procedia Technol.***, vol. 11, pp. 141–146, (2013).

[19] Mahapatra, S., Daniel, R., Dey, D. N., and Nayak, S. K., “Induction motor control using PSO-ANFIS,” ***Procedia Comput. Sci.***, vol. 48, pp. 753–768, (2015).

[20] Abd Ali, J., Hannan, M. A., Mohamed, A., and Abdolrasol, M. G. M. “Fuzzy logic speed controller optimization approach for induction motor drive using backtracking search algorithm,” ***Measurement***, vol. 78, pp. 49–62, (2016).

[21] Hannan, M. A., Ali, J. A. Mohamed, A., Amirulddin, U. A. U. Tan, N. M. L., and Uddin, M. N., “Quantum-behaved lightning search algorithm to improve indirect field-oriented Fuzzy-PI control for IM drive,” ***IEEE Trans. Ind. Appl.***, vol. 54, no. 4, pp. 3793–3805, (2018).

[22] Costa, B. L. G., Graciola, C. L., Angélico, B. A., Goedtel, A. and Castoldi, M. F. “Metaheuristics optimization applied to PI controllers tuning of a DTC-SVM drive for three-phase induction motors,” ***Appl. Soft Comput.***, vol. 62,

pp. 776–788, (2018).

[23] Purwanto, E., *et al.*, "Implementation of genetic algorithm for induction motor speed control based on vector control method," **in *2019 International Seminar on Research of Information Technology and Intelligent Systems (ISRITI)***, pp. 244–247, (2019).

[24] Hasan, F. A., Humod, A. T. and Rashad, L. J. "Robust decoupled controller of induction motor by combining PSO and Kharitonov's theorem," ***Eng. Sci. Technol. an Int. J.***, vol. 23, no. 6, pp. 1415–1424, (2020).

[25] Raj, A., Khan, Y. A. and Verma, V. "Comparative Evaluation of PSO, TLBO, and JAYA based Adaptive PI and FOPI Controllers for Vector Controlled Induction Motor Drive," **in *2021 IEEE 4th International Conference on Computing, Power and Communication Technologies (GUCON),*** pp. 1–6, (2021).

[26] Hasan, M. M., Hussain, M. S., Rana,M. S., and Roni, M. H. K. "Population Extremal Optimization Based 2-DOF Control Strategy for Field Oriented Control of Induction Motor," **in *2021 3rd International Conference on Electrical & Electronic Engineering (ICEEE)***, pp. 117–120, (2021).

[27] Mahfoud, S., Derouich, A., Iqbal, A., and Ouanjli, N. El "ANT-colony optimization-direct torque control for a doubly fed induction motor: An experimental validation," ***Energy Reports,*** vol. 8, pp. 81–98, (2022).

[28] Bojoi, R. Guglielmi, P. and Pellegrino, G.-M. "Sensorless direct field-oriented control of three-phase induction motor drives for low-cost applications," ***IEEE Trans. Ind. Appl.***, vol. 44, no. 2, pp. 475–481, (2008).

[29] Patra, N. "Study of Induction motor drive with Direct Torque Control scheme and Indirect Field Oriented control scheme with Space Vector Modulation," ***PhD diss.,*** (2013).

[30] Shang, Z. "Simulation and Experiment for Induction Motor Control Strategies," ***Electronic Theses and Dissertations, 5387,*** (2011).

[31] Farasat, M., and Karaman, E., "Speed sensorless electric vehicle propulsion system using hybrid FOC-DTC induction motor drive," **in *2011 International Conference on Electrical Machines and Systems***, pp. 1–5, (2011).

[32] Liu, H., Zhou, Y., Jiang, Y., Liu, L., Wang, T., and Zhong, B. "Induction motor drive based on vector control for electric vehicles," **in *2005 International Conference on Electrical Machines and Systems,*** vol. 1, pp. 861–865**,** (2005).

[33] Nam, K. H. "AC motor control and electrical vehicle applications," ***CRC press***, (2018).

[34] Hughes, A., and Drury, B., "*Electric motors and drives: fundamentals, types and applications*," ***Newnes,*** (2019).

[35] Sevinc, A., "Speed sensorless control of induction motors." ***Doctoral dissertation, University of Bristol,*** (2001).

[36] Lewin, C., "New Developments in Commutation and Motor Control Techniques," ***Design News***, 2006..

[37] Boldea, I. and Nasar, S. A. "Torque vector control (TVC)-a class of fast and robust torque-speed and position digital controllers for electric drives," ***Electr. Mach. power Syst.***, vol. 15, no. 3, pp. 135–147, (1988).

[38] BT, V. G., "Comparison between direct and indirect field oriented control of induction motor," ***Int. J. Eng. Trends Technol,*** vol. 43, no. 6, pp. 364–369, (2017).

[39] Kakodia, S. K., and Dynamina,G., "A comparative study of DFOC and IFOC for IM drive," **in** ***2020 First IEEE International Conference on Measurement, Instrumentation, Control and Automation (ICMICA)***, pp. 1–5, (2020).

[40] Mohammed, L. M. "Control and Analysis of a Three Phase Induction Motor By Using Stm32," ***Master's thesis, Firat University***, (2021).

[41] Liang, W., Wang, J. Luk, P. C.-K., Fang, W., and Fei, W., "Analytical modeling of current harmonic components in PMSM drive with voltage-source inverter by SVPWM technique," ***IEEE Trans. Energy Convers.***, vol. 29, no. 3, pp. 673–680, (2014).

[42] Guzman, H., Barrero, F., and Duran, M. J., "IGBT-gating failure effect on a fault-tolerant predictive current-controlled five-phase induction motor drive," ***IEEE Trans. Ind. Electron.***, vol. 62, no. 1, pp. 15–20, (2014).

[43] Hannan, M. A., *et al.*, "A quantum lightning search algorithm-based fuzzy speed controller for induction motor drive," ***IEEE Access***, vol. 6, pp. 1214–1223, (2017).

[44] Hannan, M. A. Abd Ali, J. Ker, P. J. Mohamed, A. Lipu, M. S. H. and Hussain, A. "Switching techniques and intelligent controllers for induction motor drive: Issues and recommendations," ***IEEE access,*** vol. 6, pp. 47489–47510, (2018).

[45] Gor, C., and Shah, V., "Dynamic Performance Enhancement and Comparative Analysis of Fault Tolerant Five Phase Induction Motor using PSO and GWO Algorithms" ***International Journal of Engineering Research and Technology***, vol. 13, no. 9, pp. 2318-2331, (2020).

[46] Fethia, H. Abdelhalim, T., Amel, A., Ahmed, M., and Seghir, B. M. “Tuning gain of PI controller based on Meta-heuristic techniques,” **in *2018 International Conference on Applied Smart Systems (ICASS)***, pp. 1–6, (2018).

[47] Ramli, S. S. . Mohd Sobani, N; “Jurnal Teknologi,” ***J. Teknol.***, vol. 2, pp. 19–25, [Online]. Available: www.jurnalteknologi.utm.my.(2013),

[48] Marouane, R., and Malika, Z., “Particle swarm optimization for tuning PI controller in FOC chain of induction motors,” **in *2018 4th International Conference on Optimization and Applications (ICOA)***, pp. 1–5 , (2018).

[49] Luo, Y.-C., Ke, Z.-S., and Kuo, Y.-P., “Sensorless rotor-field oriented controlled induction motor drive with particle swarm optimization algorithm speed controller design strategy,” ***Math. Probl. Eng***., vol. 2014, (2014).

[50] Hameed, I. A., Bye, R. T., and Osen, O. L., “Grey wolf optimizer (GWO) for automated offshore crane design,” **in *2016 IEEE symposium series on computational intelligence (SSCI)***, pp. 1–6, (2016).

[51] M. Jamadi and F. Merrikh-Bayat, “New method for accurate parameter estimation of induction motors based on artificial bee colony algorithm,” ***arXiv Prepr. arXiv1402.4423***, (2014).

[52] Karaboga, D., and Akay, B., “A comparative study of artificial bee colony algorithm,” ***Appl. Math. Comput.***, vol. 214, no. 1, pp. 108–132, (2009).

[53] Arshad, M. H., Abido, M. A., Salem, A., and Elsayed, A. H., “Weighting Factors Optimization of Model Predictive Torque Control of Induction Motor Using NSGA-II with TOPSIS Decision Making,” ***IEEE Access,*** vol. 7, pp. 177595–177606, (2019).

[54] Fretes, H., *et al.*, “Pareto Optimal Weighting Factor Design of Predictive Current Controller of a Six-Phase Induction Machine Based on Particle Swarm Optimization Algorithm,” ***IEEE J. Emerg. Sel. Top. Power Electron.,*** vol. 10, no. 1, pp. 207–219, (2022).

RESUME

Hersh Hassan Taha ALDAWOODI was born in Tuz-Saladeen and he finished primary, intermediate, and high school in this city. After finishing school, he joined the College of Engineering, Department of Electrical at Tikrit University in 2008. Then in 2020, he started at Karabuk University Electrical and Electronics Engineering to complete his M. Sc. education.